Ninth Quarterly Report

Date of Report: *September 14, 2010*

Contract Number: DTPH56-08-T-000014

Prepared for: DOT-PHMSA

Project Title: Effect of Concentration and Temperature of Ethanol in Fuel Blends on Microbial and Stress Corrosion Cracking of High-Strength Steels

Prepared by: Colorado School of Mines and National Institute of Standards and Technology

Contact Information: Dr. *David Olson, dolson@mines.edu, Dr. Brajendra Mishra, bmishra@mines.edu, Dr. John Spear, jspear@mines.edu, Dr. Shaily Bhola sbhola@mines.edu, Luke Jain ljain@mines.edu, Chase Williamson chawillia@gmail.com, Dr. Tom Siewert, siewert@boulder.nist.gov, Dave McColskey, mccolske@boulder.gov, Timothy Weeks, timothy.weeks@nist.gov*, Dr. *Jeffrey Sowards jeffrey.sowards@nist.gov*

For quarterly period ending: *September 14. 2010,*

CONTENTS

TABLE OF FIGURES

TECHNICAL STATUS

Technical efforts for the 9th quarter have included field sampling of fuel, biofilms, and other media from fuel grade ethanol (FGE) infrastructure, chemical analysis of field samples, microbial isolation laboratory experiments, identification of viable cells grown from field samples, electrochemical characterization of corrosion parameters for E10 fuel and water systems, immersion testing of steel coupons in fuel ethanol environments for corrosion and microbiologically influenced corrosion (MIC) evaluation, multi-specimen bend testing and pitting analysis, and assembly of a fatigue crack growth rate (FCGR) reaction frame.

Field Assessment and Microbiological Characterization

FGE underground and aboveground (UST and AST) containment/storage tanks are used to capture ethanol spillage and runoff water resulting from normal operation at fueling terminals. These types of tanks were recently discovered to have experienced internal corrosion problems. A carbon steel pipe flange, removed after failure earlier this year, can be observed in Figure 1 below.

Figure 1 Corroded carbon steel pipe flange removed from the bottom of a failed ethanol spillage aboveground storage tank (AST) reported to smell like acetic acid. MIC by acetic acid bacteria is suspected to be the cause of the failure

After the failure, similar tanks were inspected and many were reported to smell like vinegar (acetic acid) and have a *pH of around four*. As microbes are known to produce acetic acid while using ethanol as a substrate, acetic acid producing microbes were presumed to be active in the ethanol spillage tanks and suspected to be responsible for the corrosion failure. Tank bottoms samples from the ethanol contact-water tanks were acquired. The microbial diversity of these samples was investigated with 16S rRNA gene sequencing. Preliminary results indicate that acetic acid bacteria grouping within the *Alphaproteobacteria* are the most abundant type of microbes in the tank bottoms of ethanol containment tanks [Figure 1]. These findings are consistent with previous findings regarding similar tanks at multiple locations suggesting acetic acid bacteria are present in environments associated with FGe. ***Acetic acid bacteria fall under a category of microbes recognized to cause MIC known as acid producing bacteria (APB).*** The environment possibly producing internal MIC in these USTs could simulate intermittent localized conditions experienced inside interstate pipelines transporting FGE. Periods of intermittent flow or pipeline downtimes could results in sections of the line exposed to stagnant water and contaminated FGE or ethanol fuel blends (EFB). During these times, microbial communities provided with ethanol fuel as a nutrient source, could flourish and produce organic acids and other harmful constituents damaging to the line. When normal pipeline operation continues, the microbes may become dormant but could quickly return with the onset of favorable conditions once again. Depending on the duration of these events, these conditions could compromise the integrity of the pipeline after a critical number of cycles.

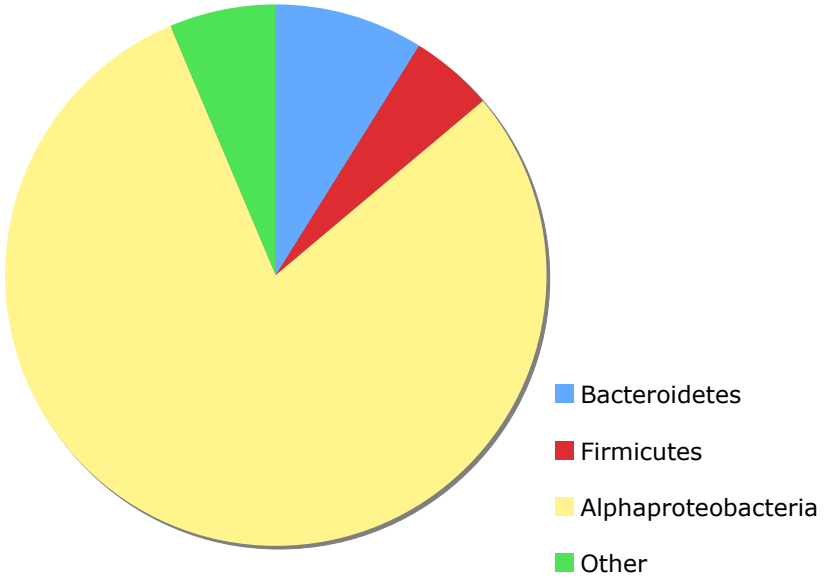

Figure 2 Microbial community composition of tank bottoms sample collected from fuel-grade ethanol (FGE) underground storage tanks (UST) containing FGE and water. *Alphaproteobacteria* representatives are comprised of acetic-acid-producing bacteria.

Laboratory Microbiological Cultivation Efforts

Several types of microbes that may potentially influence corrosion of metals have been identified via 16S rRNA gene sequencing in samples collected from commercial FGE infrastructure. Cultivation experiments have been designed to isolate and grow these potentially corrosive microbes in the laboratory. A variety of microbial growth media have been inoculated with samples collected from ethanol industry infrastructure. ***Viable cells have now been obtained from all samples, including samples collected from environments containing FGE with water concentrations under 1 pct.*** These experiments indicate that viable microbes with potentially corrosive metabolisms are present in many locations along FGE storage and transportation systems. Cultivars include acetic-acid- producing bacteria grouping with *Acetobacter* species and spore-forming bacteria grouping with *Bacillus* species. *Acetobacter* species are capable of converting ethanol to acetic acid and have been identified in ethanol containment tanks experiencing corrosion problems. *Bacillus* species have been linked to MIC, and some *Bacillus* species are known to produce spores capable of oxidizing manganese. Additional cultivars have been grown in the lab and will be identified with 16S rRNA gene sequencing. These cultivars

will continue to be evaluated to determine if their metabolic activities influence the corrosion of steels.

Laboratory immersion testing

Corrosion testing efforts have included a set of experiments designed to evaluate MIC of linepipe steel coupons in water and E10 fuel environments inoculated with microbes retrieved from the FGE spillage USTs. Eight API X70 steel coupons were placed in E10 fuel and water mixtures to evaluate pitting and corrosion. The test compared four sterile control coupons with no inoculum with four coupons inoculated with samples of aqueous media from an industrial ethanol-spillage UST containing associated microbial consortia.

All corrosion test cells were setup using appropriate aseptic procedures to ensure that the only microbes introduced into the test cells would originate from the addition of FGE spillage tank media. Jars and lids were autoclaved, soaked in 70% ethanol and exposed to ultraviolet radiation. Coupons were soaked in ethanol and flame sterilized. Creek water samples were autoclaved. E10 fuel was passed through a 0.2 um filter to remove any microbial cells present. The corrosion cells were assembled in a laminar flow hood under filtered air, sealed after immersion, and remained sealed for the testing duration. Testing conditions are listed below in Table I.

Table I Test Matrix for API X70 Two-phase E10 fuel/creek water MIC Immersion Testing

	Specimen			Environment				
	Material	Dimensions	Weight	Creek Water	E10	Innoculum (SC)	Test Duration	pH (final)
[#]	[type]	[in]	[g]	[ml]	[ml]	[ml]	[days]	
1	API X70	1 X 1 X 0.1875	24.2880	20	60	0	2	6.5
2	API X70	1 X 1 X 0.1875	24.1544	20	60	0	5	6.75
3	API X70	1 X 1 X 0.1875	24.2625	20	60	0	8	6.5
4	API X70	1 X 1 X 0.1875	24.3373	20	60	0	45	6.5
5	API X70	1 X 1 X 0.1875	24.3076	20	60	1	2	5.5
6	API X70	1 X 1 X 0.1875	24.2912	20	60	1	5	5.25
7	API X70	1 X 1 X 0.1875	24.1356	20	60	1	8	5.25
8	API X70	1 X 1 X 0.1875	24.3214	20	60	1	45	5.25

After one day of immersion, brown solids were observed to form at the organic/aqueous interface of the inoculated jars. After two days of immersion, an increased amount of red/brown debris was observed in the inoculated jars when compared to the control, however, there seemed to be more corrosion product near the coupons in the control test cells. The increased amount of

debris located near the liquid interface could be to due to the activity of microbes. Microbes associated with MIC are known to proliferate while residing in the aqueous phase and utilizing an adjacent organic (E10) phase as a source of carbon and other organic nutrients. The reason for the increased corrosion product near the coupons in the control test cells could be due to the higher pH of these cells and corresponding lower iron solubility. Upon removal of Coupons 1 and 5, it was observed that there was more particulate matter in the aqueous layer of Sample 5 than in the aqueous layer of Sample 1. During the removal of Coupons 2 and 6, it was also observed that there was an increased amount of red/brown debris in the inoculated jars but more corrosion product near the coupons in the control test cells. When Coupons 3 and 7 were removed, it was observed that the organic/aqueous interface of the inoculated Sample contained orange particulates. The interface of the control test cell contained less debris but was a darker brown color. The inoculated Coupon 7 had a smooth, uniform layer of corrosion product on the surface while the control had a thick and uneven orange product.

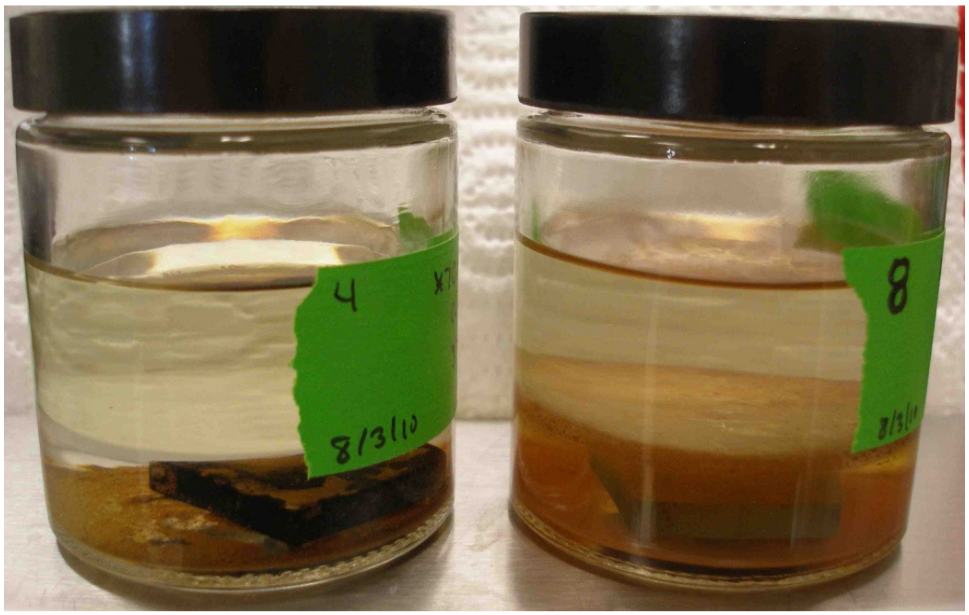

Figure 3 API X70 steel Coupons 4 and 8 immersed in the aqueous phase (lower layer) beneath the E10 fuel (upper layer). The jar on the left in Figure 3 is a sterile control. The jar on the right is inoculated with the tank bottoms sample. The microbial consortium in the tank bottoms sample is known to include acetic-acid-producing bacteria (APB) and possibly sulfate reducing bacteria (SRB)

Upon inspection of Jars 4 and 8, it was observed that a significant amount of debris was present at the interface of Sample 8 as shown above in Figure 3. Significant quantities of debris were also observed to be present on the bottom of the jar. The aqueous layer of Sample 8 appeared to be more turbid than Sample 4. Sample 4 was observed to be free of debris at the aqueous/organic interface and was observed to have less debris on the bottom of the jar. The corrosion on Coupon 4 was observed to be darker and less even than on Coupon 8. Coupon 8 was observed to have a thick even reddish coating of corrosion product. Closer inspection of the coupons after removal from the test cell revealed the presence of four large pits covered with black corrosion product as shown in Figure 4. Orange/brown as well as black deposits can be indicators of the activity of sulphate reducing bacteria SRB and/or iron oxidizing bacteria (IOB) (Blackburn 2004). The pits were broad, shallow, and had a stadium like morphology characteristic of MIC pits formed by a localized environment commonly produced by SRB. It should be noted that while pit morphology may be indicative of MIC, it should not be used as the sole indicator (Javaherdashti 2008).

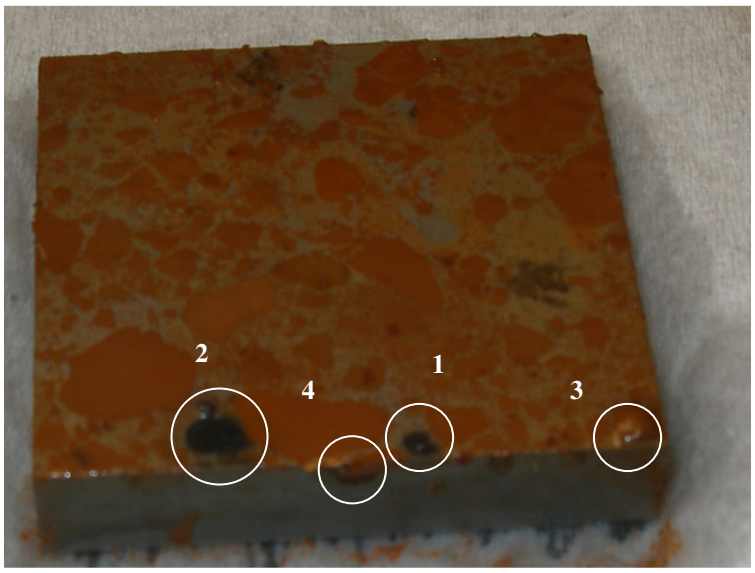

Figure 4 Photograph of pitted API X70 steel coupon (1 inch X 1 inch X 0.1875 inch) #8 removed from the aqueous volume of a two-phase system containing autoclaved creek water and filtered E10 fuel after 45 days of immersion displaying orange/brown corrosion product and four distinct corrosion pits (pre-washing)

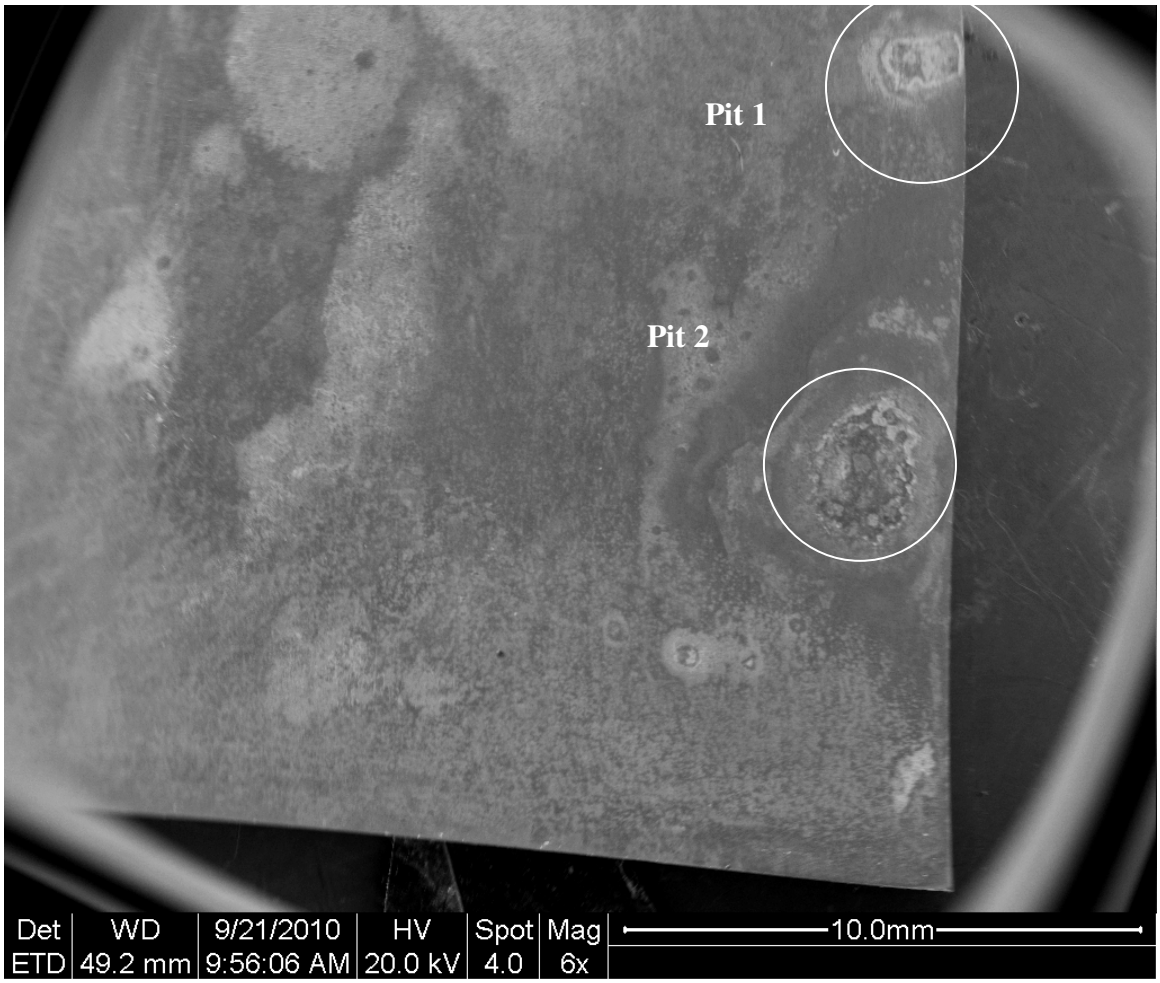

Figure 5 Environmental scanning electron microscopy (ESEM) micrograph of pitted API X70 steel coupon (1 inch X 1 inch X 0.1875 inch) #8 removed from the aqueous volume of a two-phase system containing autoclaved creek water and filtered E10 fuel after 45 days of immersion showing corrosion pits (6x)

The environmental scanning electron micrograph (ESEM) in Figure 5 shows pits 1 and 2 on X70 coupons 8. The ESEM image in Figure 6 shows a further magnified pit number 2 on X70 steel coupon eight. The entire pitted area partially covered by scale is depicted in the Figure. The area in the center of the pit still mostly covered with oxide is also indicated. Energy dispersive X-ray spectroscopy (EDS) was used for elemental analysis of locations in the pitted region. While EDS yields the elemental composition of the material, it does not give information about the bonding state (elemental form) or concentration of the elements present. EDS spot analysis was performed at several locations in the pitted area to search for elemental indicators of

microbial activity or MIC. The presence of sulphur, manganese, carbon, calcium, and/or phosphorous can be indicative of MIC.

In the region of the pit where the oxide had been removed, EDS generated primary iron peaks collaborating with the visual observation that the oxide had been removed in this region exposing the metallic base of the pit. EDS spot analysis of the darker grey areas in the central region of the pit yielded strong iron and oxygen peaks confirming the presence of a relatively thick layer of iron oxide. Most interestingly, it was often the case that when EDS spot analysis was performed at locations near the border of the oxide covering (locations 4, 7, 8, 9), the presence of sulphur and carbon was more pronounced. Sulphur is of interest as sulphate-reducing bacteria (SRB) are known to metabolize sulfates by reducing them to sulphide. The resulting sulfide can be found deposited on the surface of the corrosion site in the form of iron sulphide. Carbon signals were also observed to be present in the EDS spectra that demonstrated the presence of sulphur. These peaks may also suggest the presence of organic material (e.g. extracellular polymeric substance, microbial cells) and corresponding microbes at the corrosion site. The size of the peaks appeared to be somewhat proportional with larger sulphur peaks corresponding to larger carbon peaks.

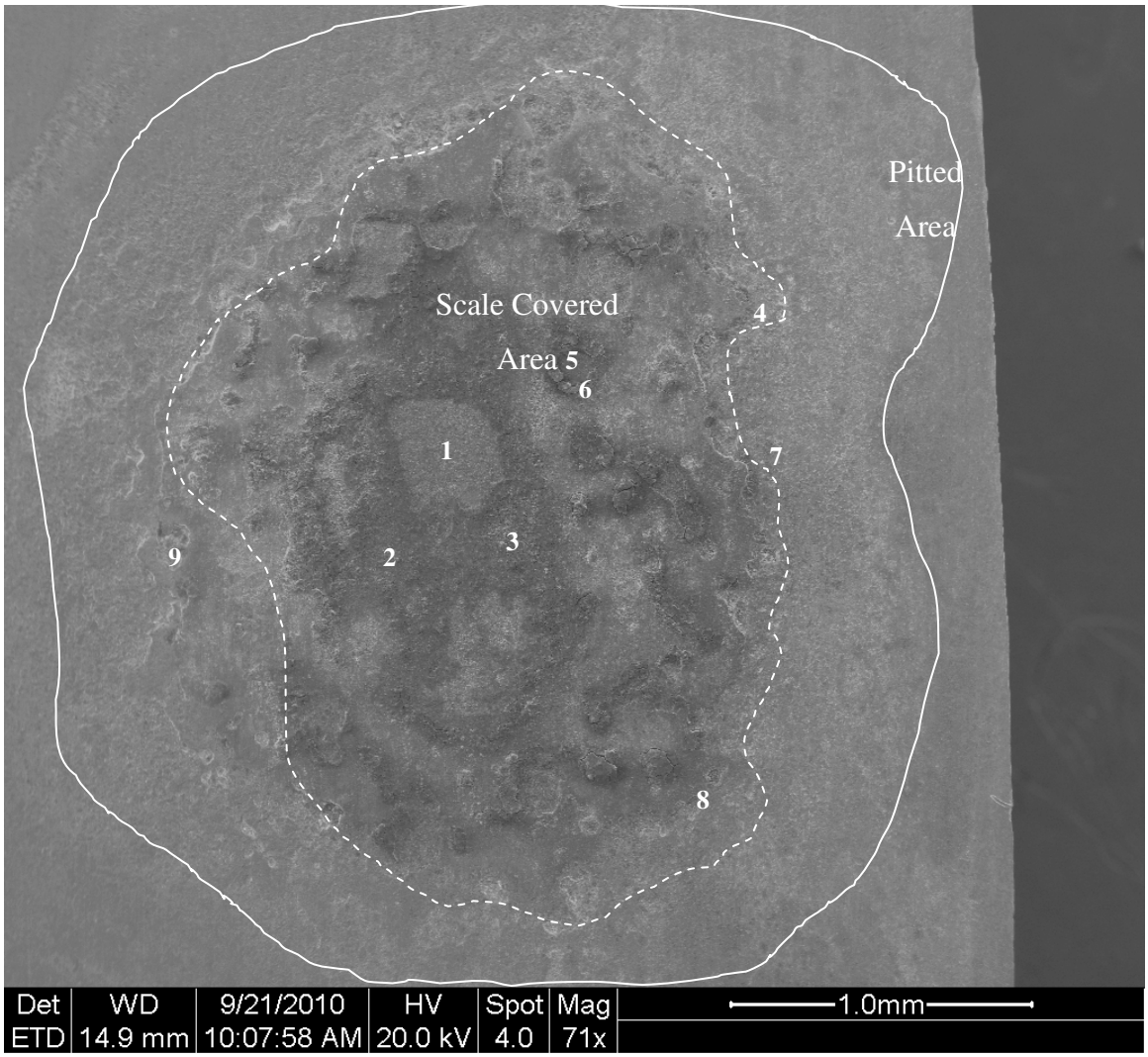

Figure 6 Environmental scanning electron microscopy (ESEM) image of pit number 2 with pitted area bounded by a solid white line, the area of general scale cover bounded by a dashed white line, and numbered energy dispersive X-ray spectroscopy (EDS) spot analysis locations (1-9) (71x)

EDS spot analysis of locations 1 and 5 are shown in Figure 7. The presence of large iron peaks along with the absence of significant signals of any other elements indicates that the base of the pit, where it is not covered by scale, is most likely predominately composed of elemental iron.

Figure 8a depicts an EDS spot analysis performed on area 3 in a region of the pit still covered in scale. Strong iron and oxygen signals, along with significant sulphur and carbon peaks indicate that the scale is largely composed of iron oxide but also contains sulphur and carbon. Figure 8b

displays EDS spot analysis of location 4. Strong iron peaks and sizable oxygen peaks are present. Larger carbon and sulphur peaks can also be observed. The presence of sulphur and carbon in the scale of a pit can indicate MIC.

Locations 2 and 6 comprise areas of the pit still covered by scale. Location 2 represents one of the largest regions of an intact scale deposit. Figure 9a shows very large iron and oxygen signals corresponding with this area indicating that the scale most likely has significant concentrations of iron oxide. A small sulphur peak is also visible indicating the possible presence of iron sulphide or other sulphur species. Location 6 also represents an area covered in scale yet very close to location 5, which is free of scale. The EDS spot analysis of this location yields a strong iron signal and a significant oxygen signal. A somewhat smaller sulphur peak is also observed. This most likely indicates metallic iron, iron oxide, and some sulphur compound, possibly an iron sulphide.

Areas 7 and 8 are located on the edge of the intact scale in the central region of the pit. These areas were of particular interest. Along with the expected presence of iron and oxygen, relatively large carbon and sulphur signals were also commonly observed. These signals can be seen in especially in Figure 10a and also in Figure 10b. A small but noticeable manganese signal should also be noted in Figure 10b. Manganese oxide is associated with manganese oxidizing bacteria and known to be present in zones of MIC (B. J. Little 2006).

Area 9 is also located on the edge of the intact scale in the central region of the pit. Again, in addition to a strong iron signal, a large sulphur peak is present.

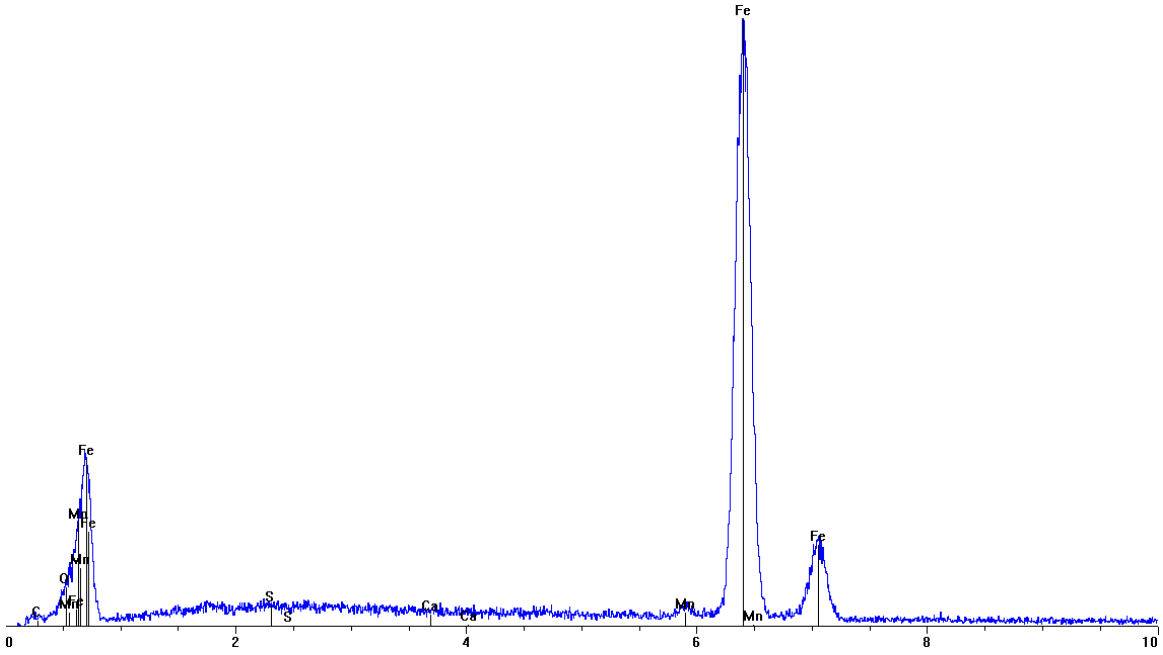

(a)

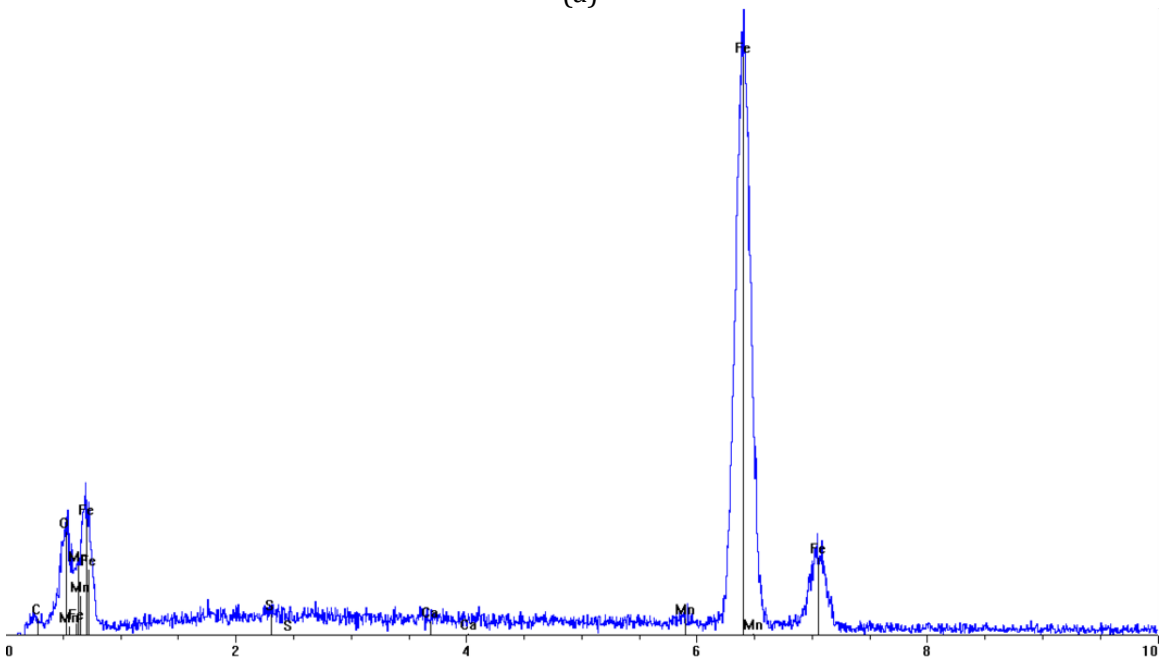

(b)

Figure 7 Energy dispersive X-ray spectroscopy (EDS) spot analysis at 20 kV of (a) location "1" showing predominantly iron peaks indicating metallic iron (b) location "2" showing iron and oxygen peaks indicating iron oxide

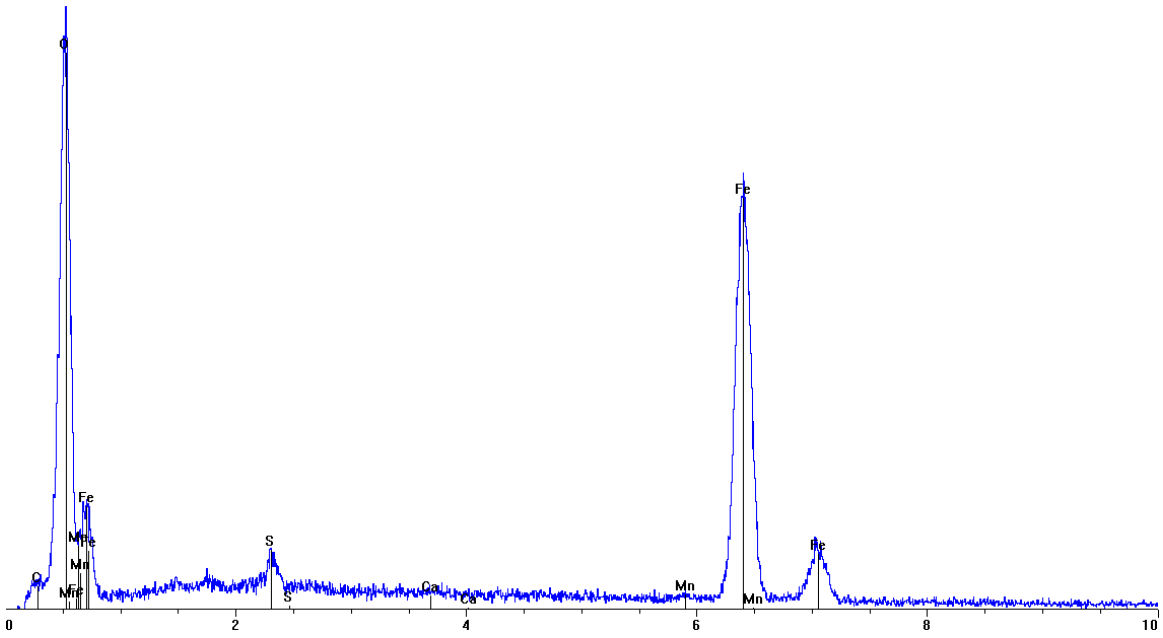

(a)

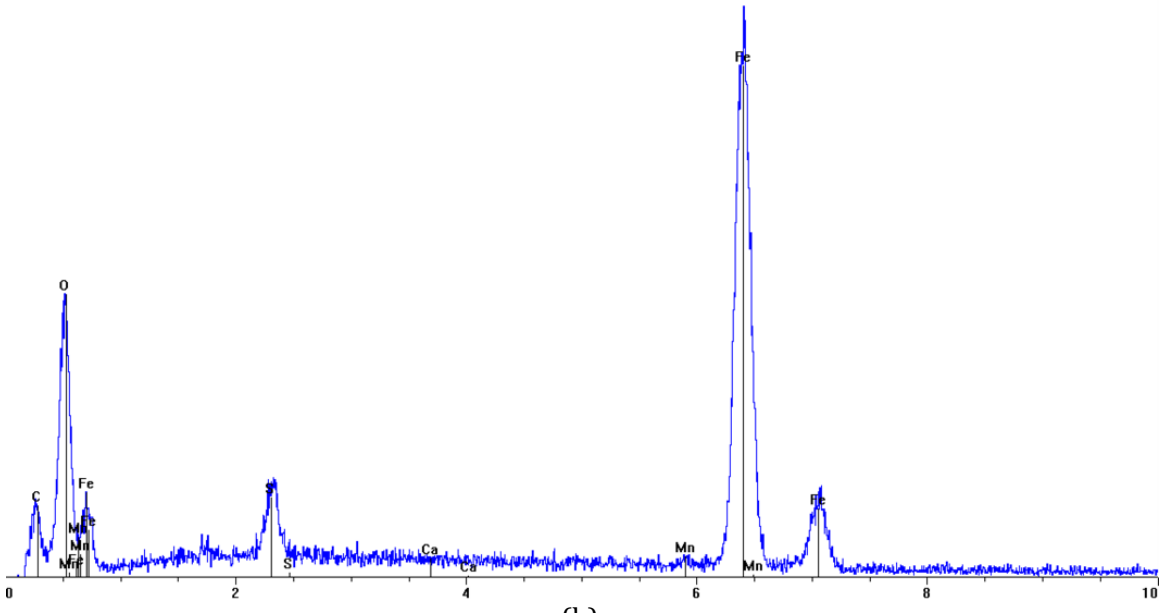

(b)

Figure 8 Energy dispersive X-ray spectroscopy (EDS) spot analysis at 20 kV of (a) location "3" showing iron and oxygen peaks indicating iron oxide with some amount of sulfur species (b) location "4" depicting large iron and oxygen peaks as well as smaller carbon and sulphur peaks indicating iron oxide with some amount of both sulfur and carbon species

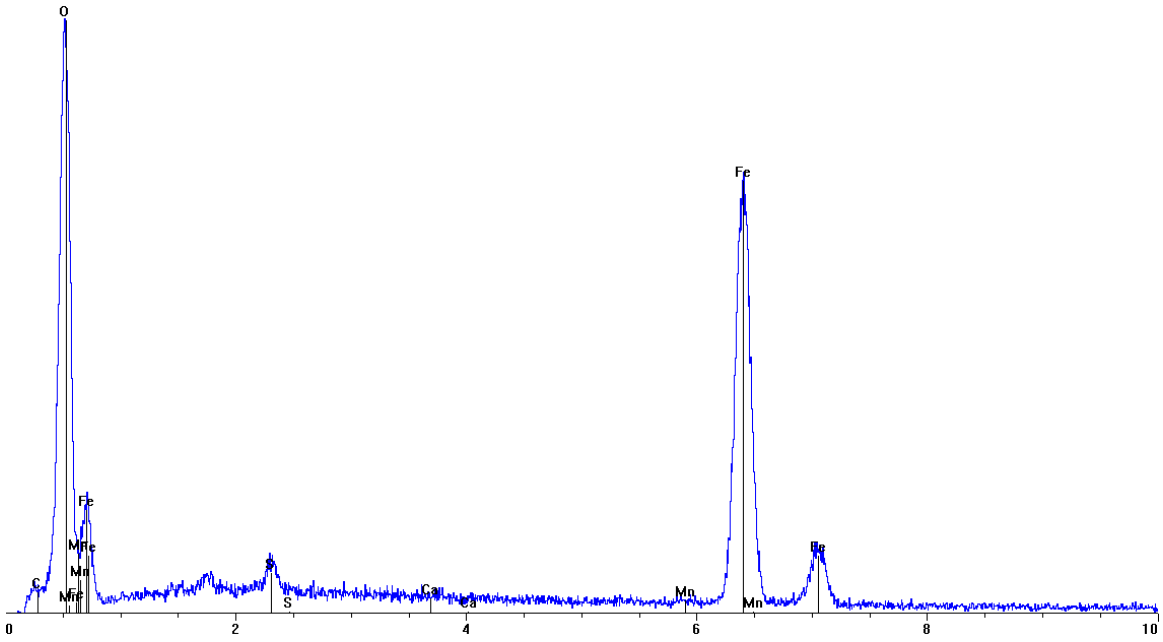

(a)

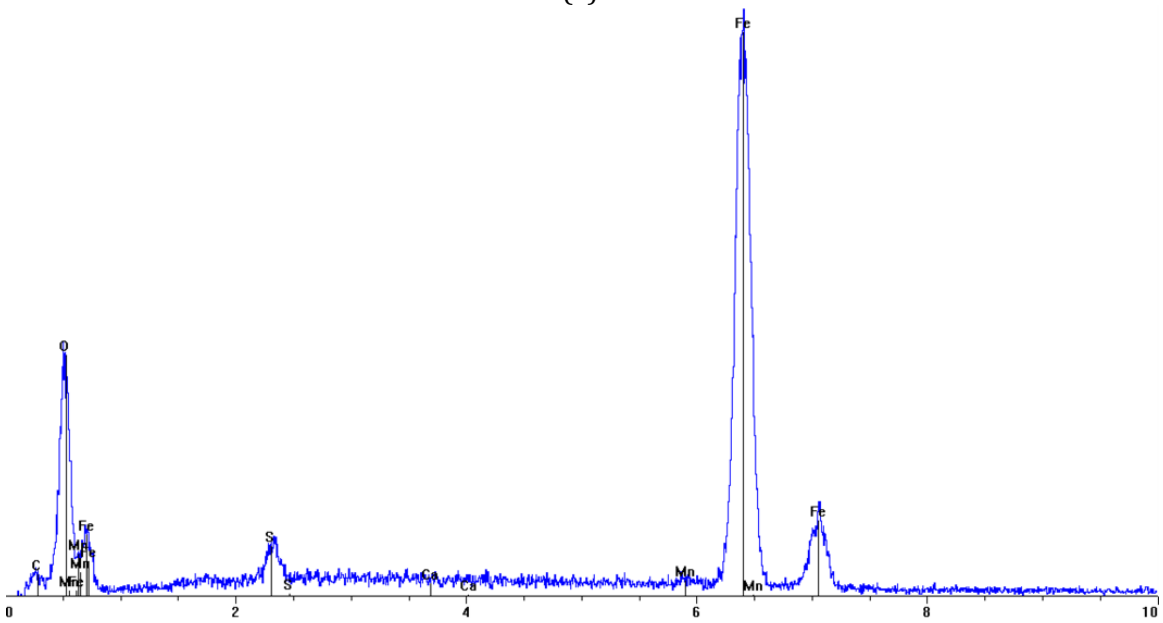

(b)

Figure 9 Energy dispersive X-ray spectroscopy (EDS) spot analysis at 20 kV of (a) location 5 showing predominantly iron peaks indicating metallic iron (b) location 6 showing large iron and oxygen peaks and a smaller sulphur peak indicating the presence of iron oxide as well as some sulphur

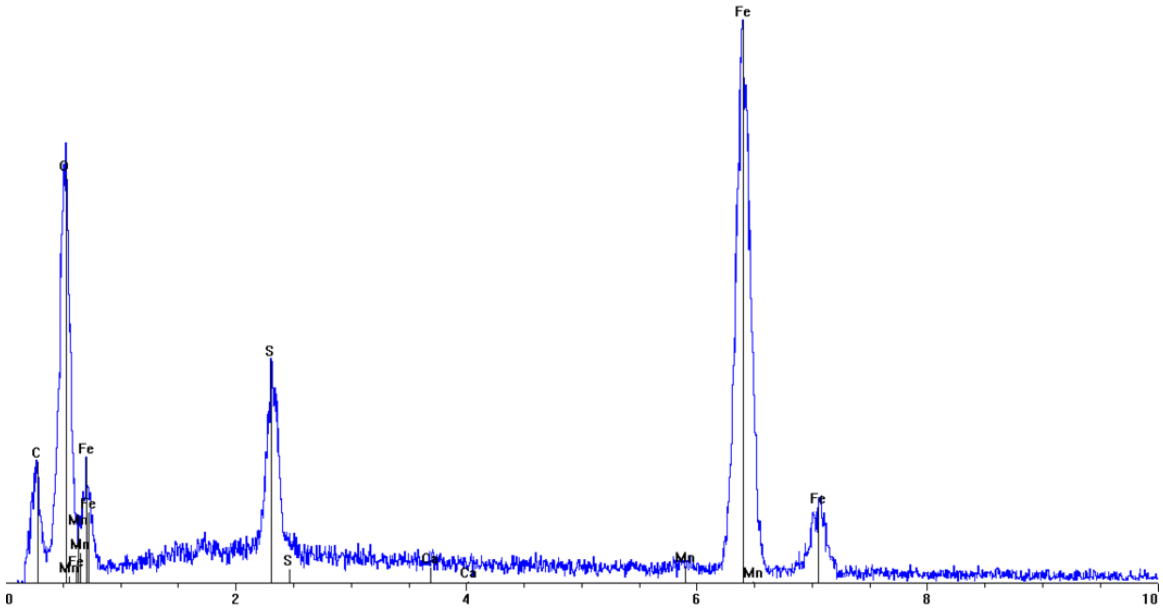

(a)

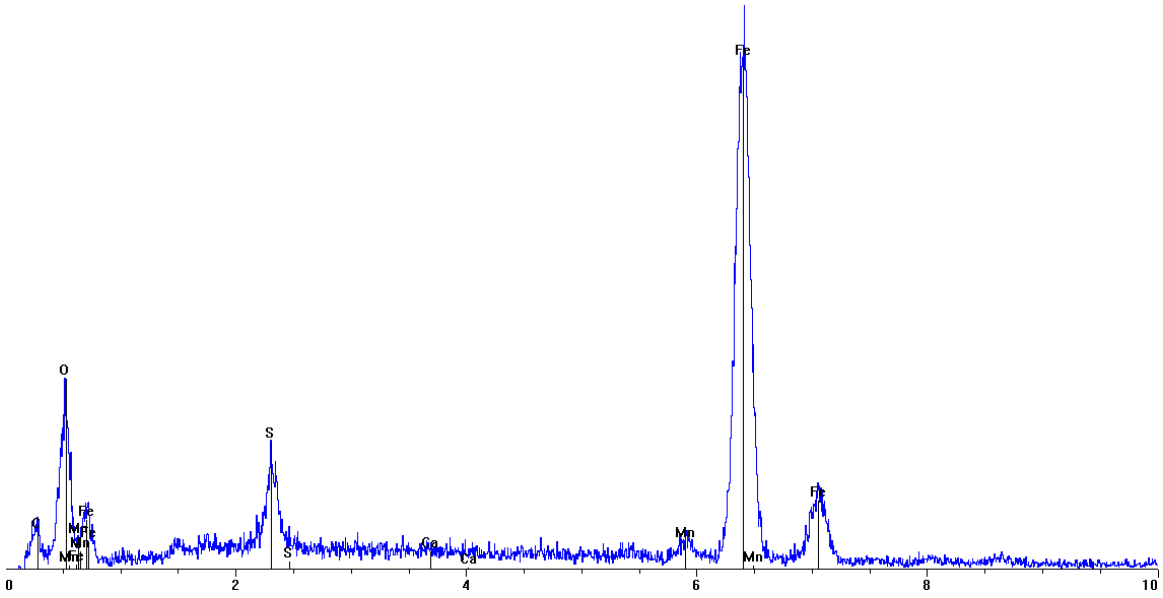

(b)

Figure 10 Energy dispersive X-ray spectroscopy (EDS) spot analysis at 20 kV of (a) location 7 showing large iron, oxygen, and sulphur peaks as well as a carbon peak indicating iron oxide, a sulphur species, and some form of carbon (b) location 8 showing large iron as well as smaller oxygen, sulphur, and carbon peaks indicating metallic iron as well as some oxide, sulphur, and carbon and a smaller sulphur peak indicating the presence of iron oxide as well as some sulphur

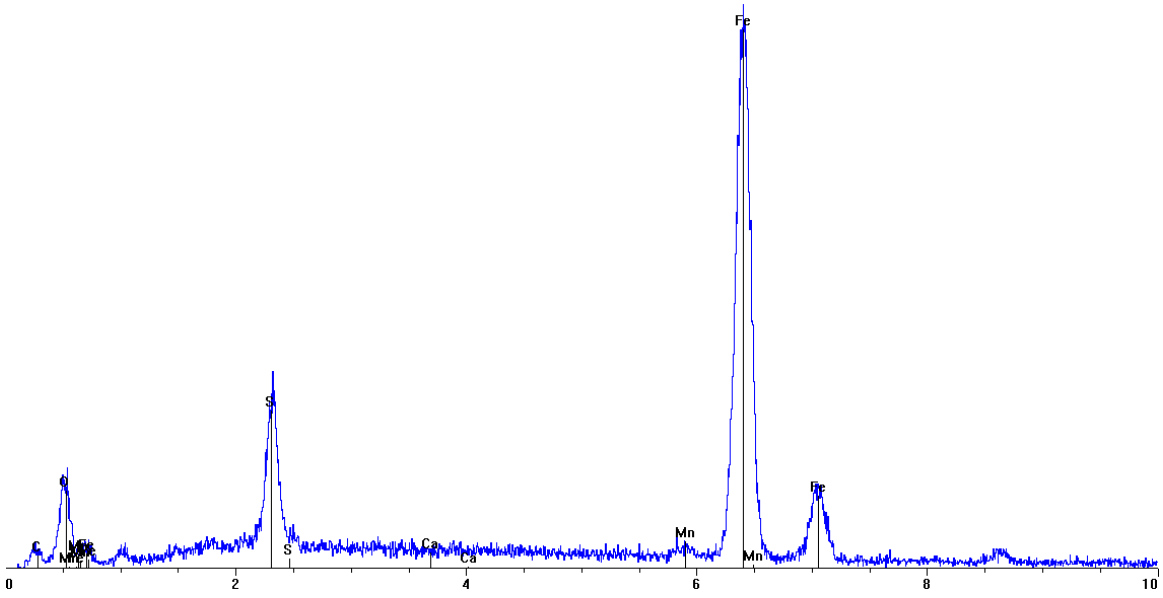

Figure 11 Energy dispersive X-ray spectroscopy (EDS) spot analysis at 20 kV of location 9 showing large iron and sulphur peaks as well as a small oxygen peak indicating the presence of iron as well as some concentrations of oxygen and sulphur species

Due to the presence of large sulphur and carbon peaks found at location 7 in pit 2, a more detailed investigation was performed in that area. Several ESEM micrographs were acquired of the area at different magnifications as shown below in Figure 12. The area is located to the right of the center of the pit approximately one half of the distance to the outer rim. This area is also observed to be approximately where the scale covering over the pit base ends. Upon closer observation, morphology can be observed which does not to appear to be typical of an inorganic structure likely to be found at a sight of steel corrosion.

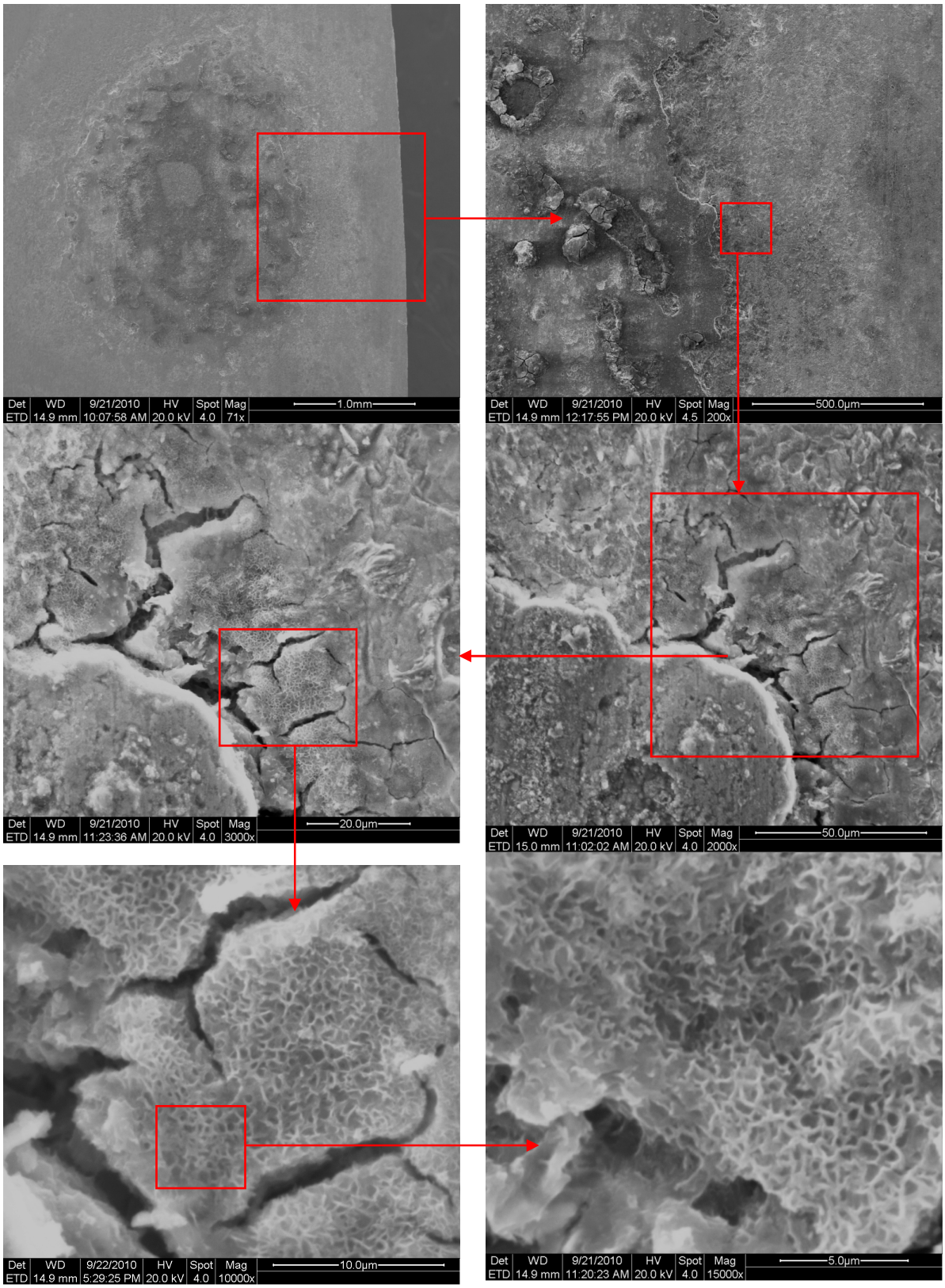

Figure 12 ESEM imaging of location seven on pit two using varying magnifications

The EDS spot analysis of location 7 on pit 2 was performed at high magnification at locations 7A-7R defined below in Figure 13. The EDS analysis of locations in the lower right corner of the image (7G and 7C) yielded strong iron and oxygen peaks indicating the prevalence of iron oxide. The analysis confirms that the center of the pit is largely covered in iron oxide. The EDS analysis of locations on the right side and upper right corner of the image depicted only large iron peaks indicating metallic iron. These results confirm that the outer edges of the pit the exposed pit bottom. The EDS spot analysis of locations (A, D, E, F, I, J) coinciding with the fibrous feature yields relatively strong sulphur and carbon signals compared with the surrounding surface. This information reinforces the possibility that the feature could be organic and associated with organisms utilizing sulphur species.

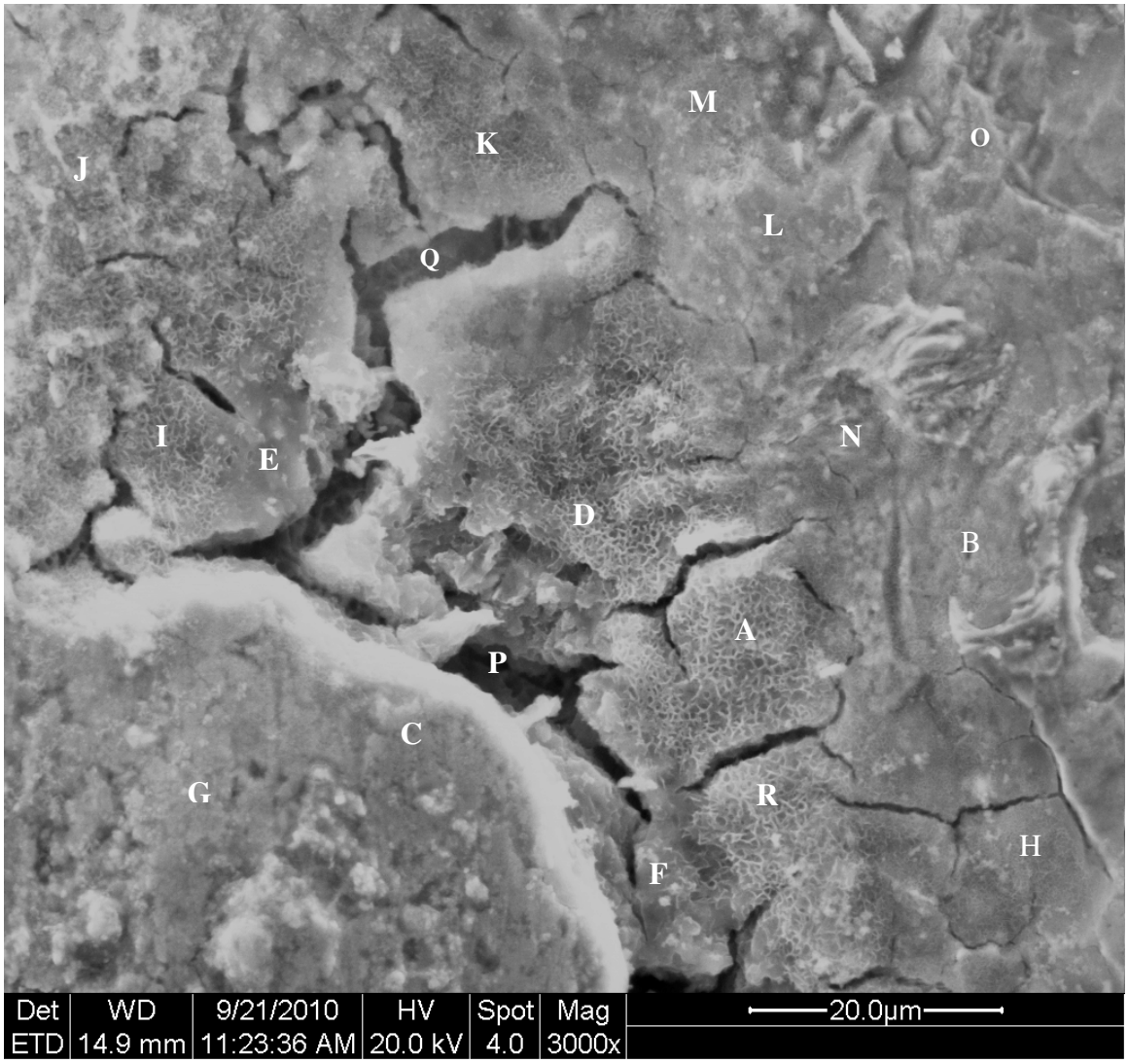

Figure 13 SEM imagine at 20 kV of location 7 on pit 2 on an API X70 steel coupon (3000x)

Locations O and N represent the right-hand side and upper right hand corner of Figure 13 showing the uncovered base of the pit. EDS spectra of these locations shown in Figure 14 demonstrate an EDS spectra characteristic of metallic iron.

Locations C and G in the lower left-hand corner of Figure 13 represent a localized area covered with intact scale. The EDS spot analysis of these areas [Figure 15] indicates the presence of iron oxide.

Locations H and K were selected to represent the intermediate area between the right side of the micrograph depicting the exposed surface of the pit and the region identified by D, A, and R showing a possibly organic morphology. The spectra in Figure 16 showing iron, oxygen, and sulphur indicate that this region may represent a transition region from metallic iron to area of suspected microbial activity.

Locations D and I are comprised of a unique morphology that may have been microbiologically generated. The EDS spot analysis of this area shown in Figure 17 supports the possibility of microbial activity as it contains strong sulphur and carbon signals when compared to other locations on Figure 13.

Locations E and F, adjacent to the suspected biofilm were also of particular interest. As shown in Figure 18 these deposit were rich in not only carbon and sulphur, but in one case [Figure 18] calcium. Calcium deposits are known to occur due to pH gradients caused by the action of microbial activities in biofilms near metallic surfaces (Videla 1992).

Locations P and Q represent areas where deep cracks appear to penetrate the surface. The EDS spot analysis in the cracks indicate the prevalence of metallic iron suggesting that the cracks penetrate into the underlying steel surface thereby exposing new surface for corrosive attack. These results may indicate microbial attack and resulting chemical dissolution, possibly along grain boundaries.

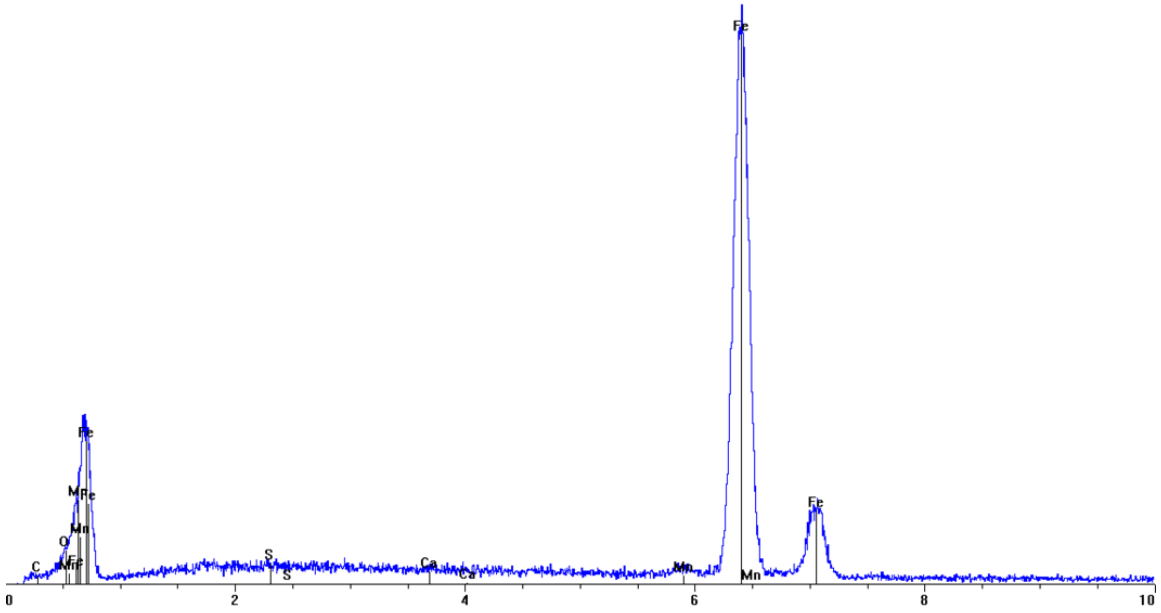

(a)

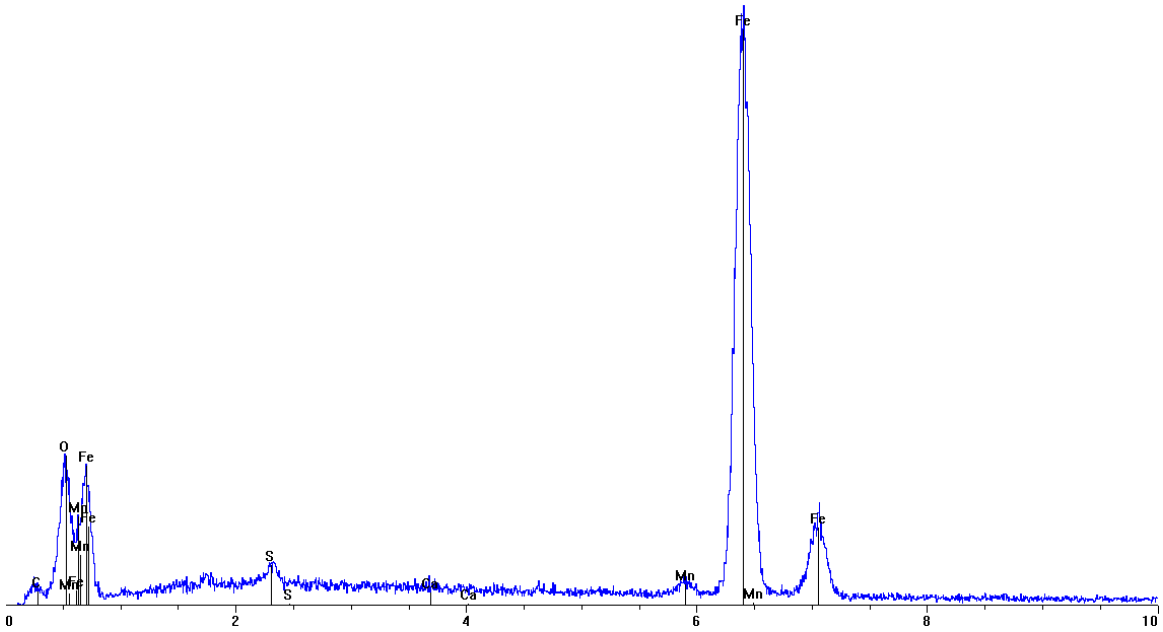

(b)

Figure 14 Energy dispersive X-ray spectroscopy (EDS) spot analysis at 20 kV depicting strong iron peaks and smaller oxygen, sulphur and manganese peaks indicating predominately metallic iron with smaller amounts of oxides, sulphur, and manganese species of an API X70 steel coupon at locations in area “7” (Figure 13) (a) “O” and (b) “N”

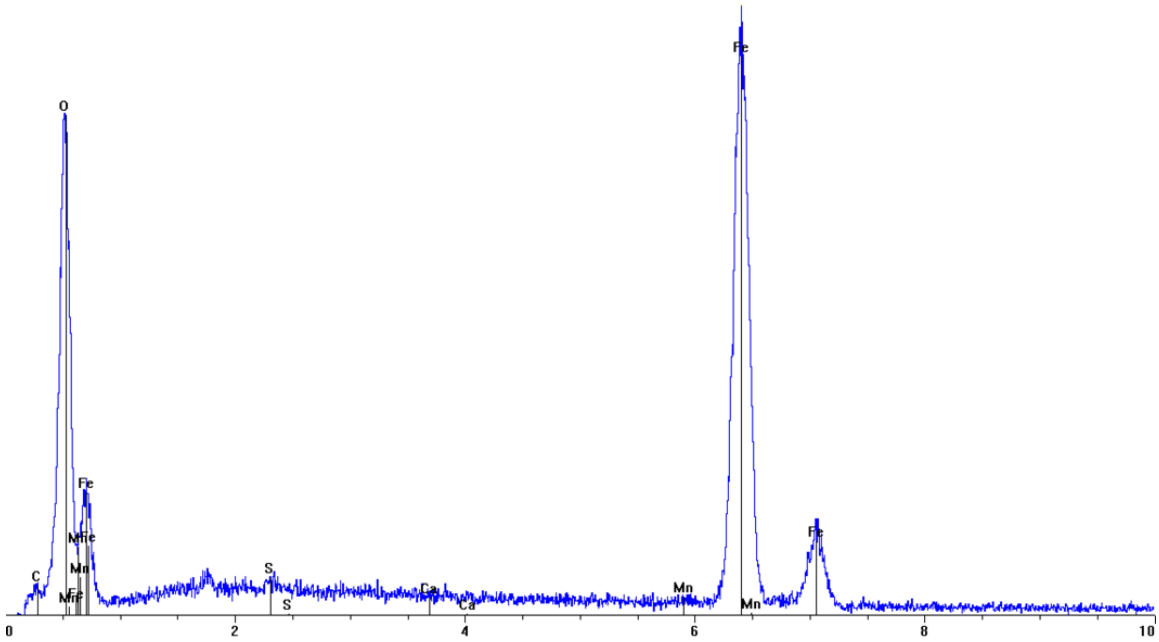

(a)

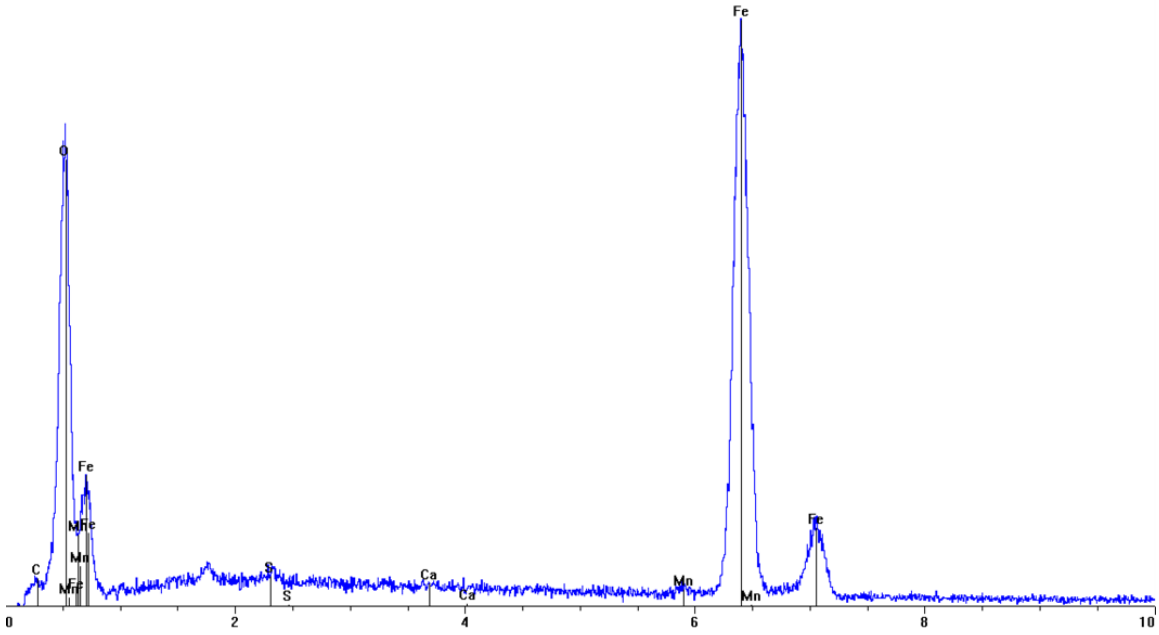

(b)

Figure 15 Energy dispersive X-ray spectroscopy (EDS) spot analysis at 20 kV depicting strong iron and oxygen peaks as well as small carbon, sulphur, and manganese peaks indicating predominately iron oxide along with the presence of carbon, sulphur, and manganese species at locations in area “7” (Figure 13) (a) “C” and (b) “G”

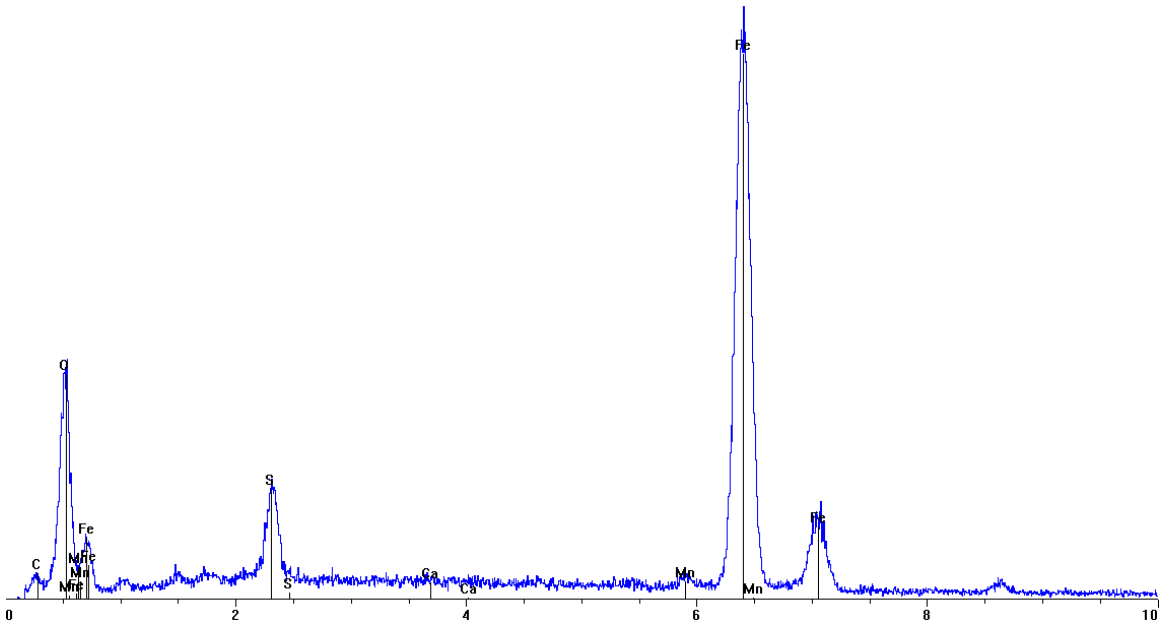

(a)

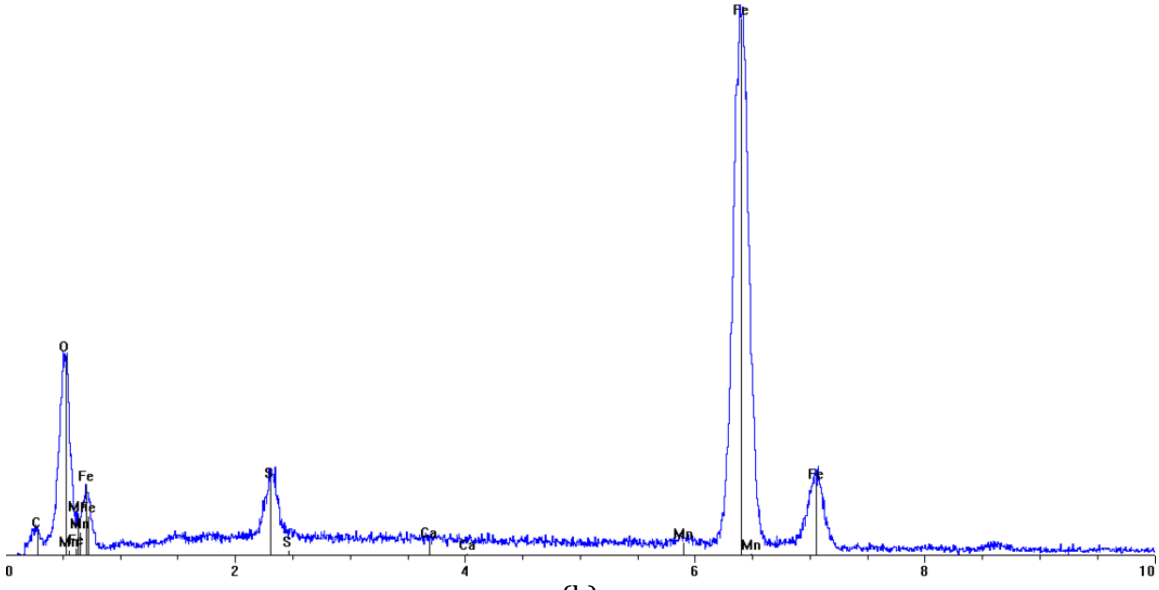

(b)

Figure 16 Energy dispersive X-ray spectroscopy (EDS) spot analysis at 20 kV depicting strong iron and oxygen peaks as well as a moderately sized sulphur peak and smaller carbon, sulphur, and manganese peaks indicating iron and iron oxide along with the presence of carbon, sulphur, and manganese species at locations in area “7” (Figure 13) (a) “B” and (b) “K”

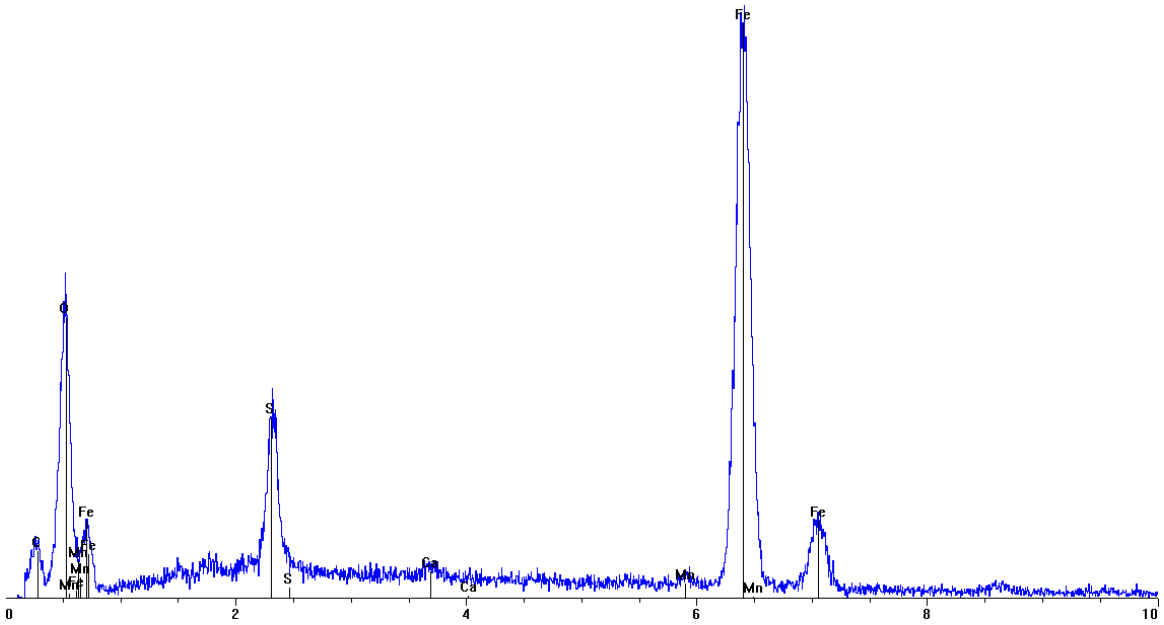

(a)

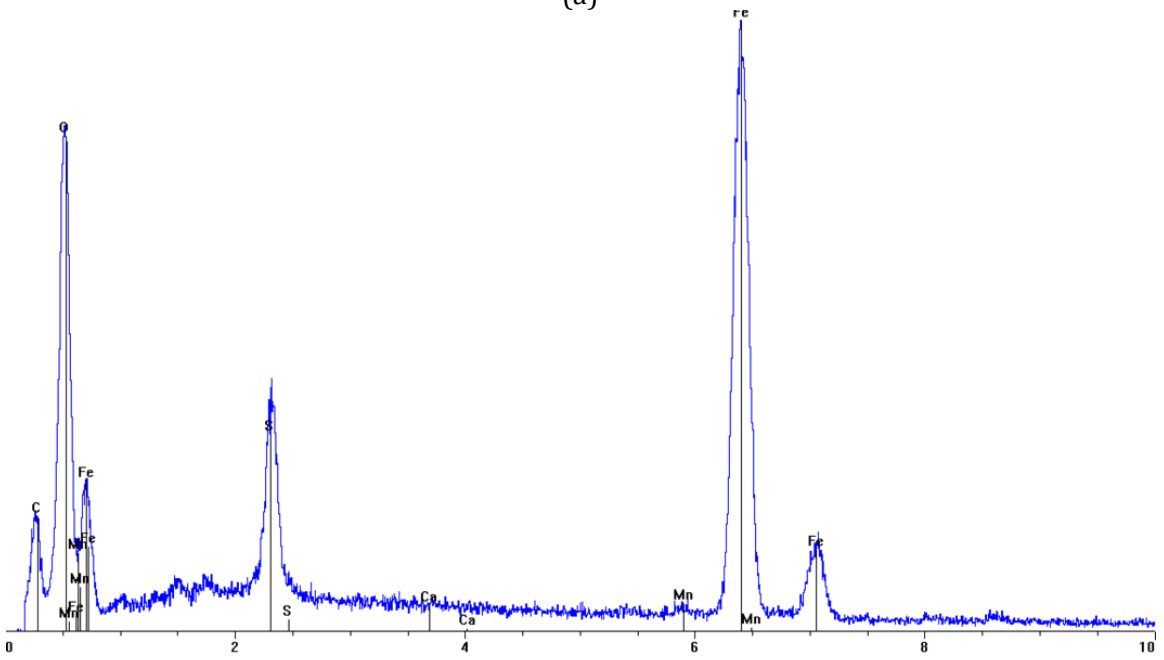

(b)

Figure 17 Energy dispersive X-ray spectroscopy (EDS) spot analysis at 20 kV depicting strong iron and oxygen peaks as well as a moderately sized sulphur and carbon peaks and slight calcium and manganese peaks indicating iron and iron oxide along with the presence of sizable quantities of carbon, sulphur, and manganese species at locations in area "7" (Figure 13) (a) "A" and (b) "I"

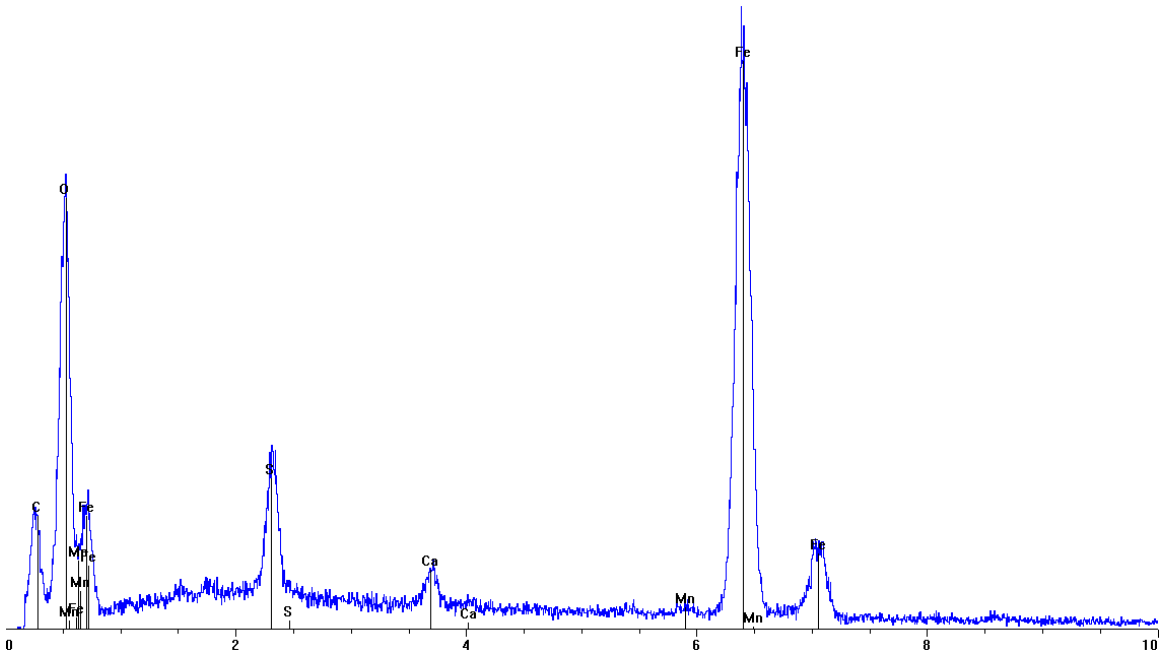

(a)

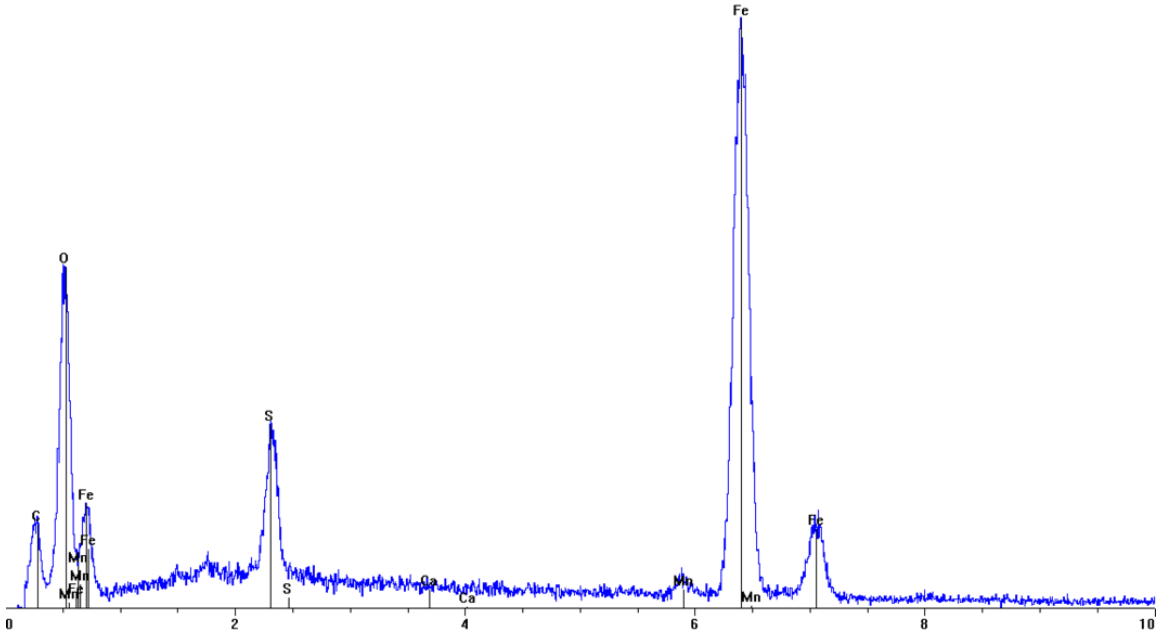

(b)

Figure 18 Energy dispersive X-ray spectroscopy (EDS) spot analysis at 20 kV depicting strong iron and oxygen peaks as well as a moderately sized sulphur, carbon, and calcium (a) peaks and slight manganese peaks indicating iron and iron oxide along with the presence of sizable quantities of carbon, sulphur, calcium and some manganese species at locations in area "7" (Figure 13) (a) "E" and (b) "F"

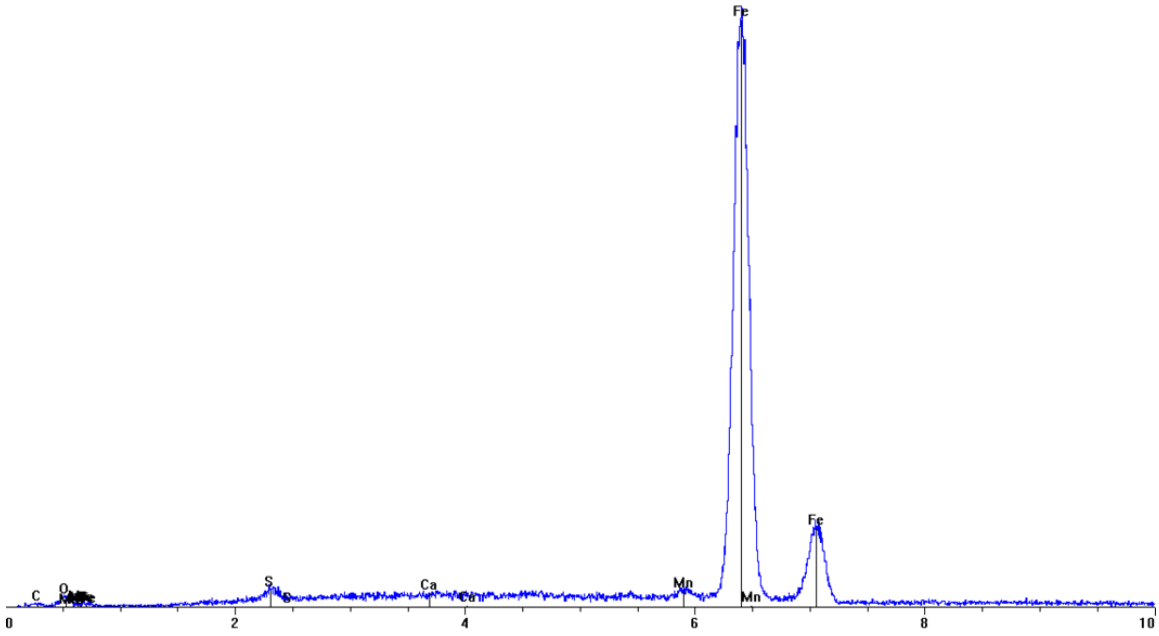

(a)

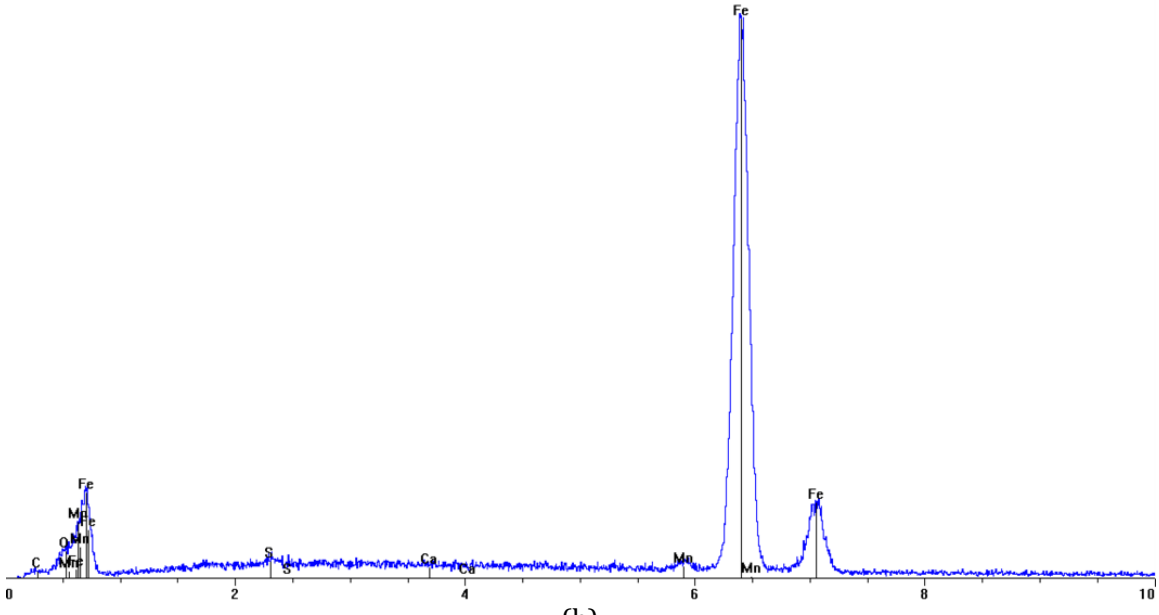

(b)

Figure 19 Energy dispersive X-ray spectroscopy (EDS) spot analysis at 20 kV depicting strong iron peaks indicating predominately metallic iron with smaller amounts of oxides, sulphur, and manganese species of an API X70 steel coupon at locations in area "7" (Figure 13) (a) "P" and (b) "Q"

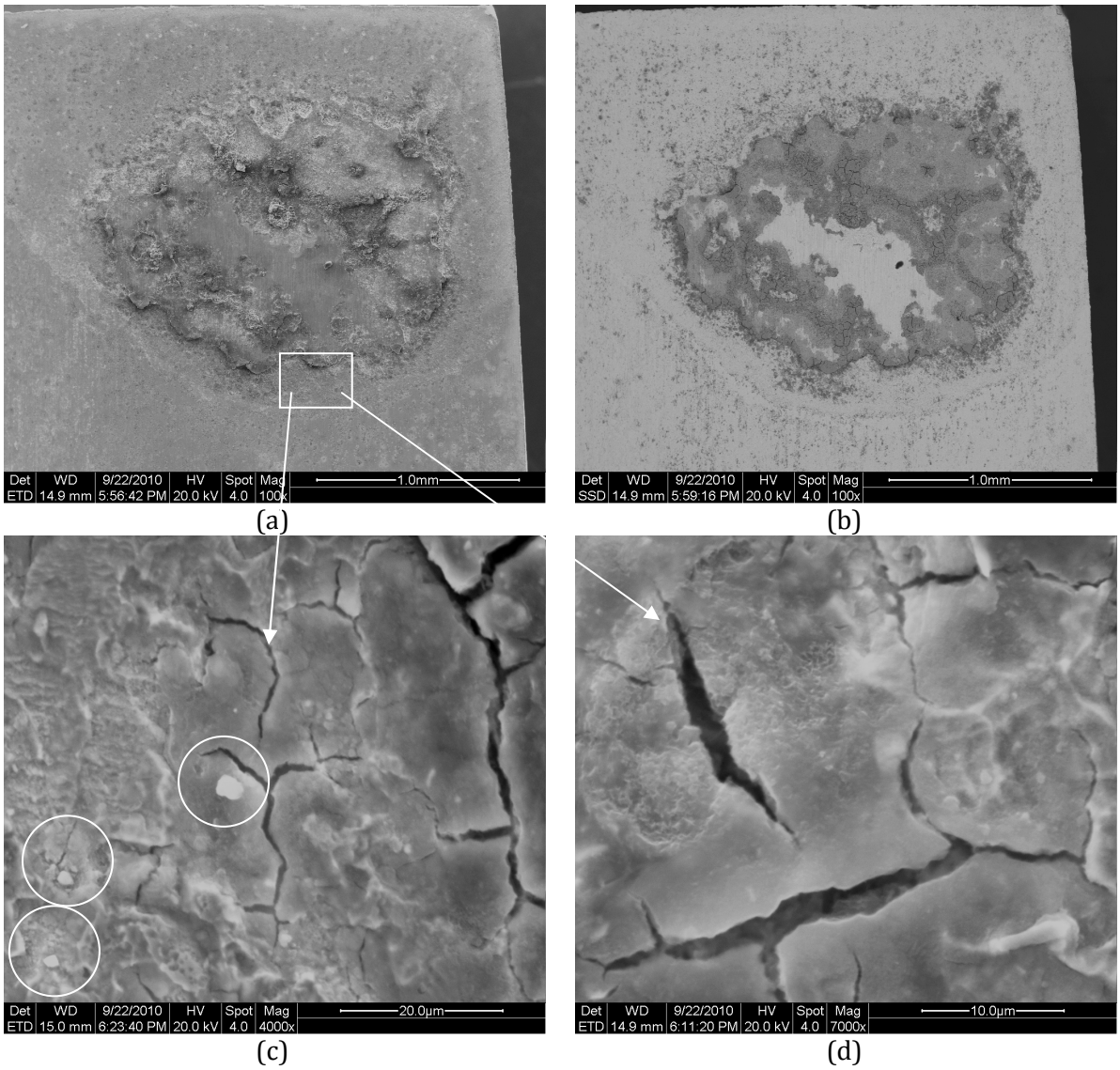

Figure 20 Environmental scanning electron microscopy (ESEM) micrographs of pit 2 on API X70 steel coupon (1 inch X 1 inch X 0.1875 inch) number 8 showing (a) a secondary electron image of the pit (100x) (b) back-scattered electron (BSE) image of the pit (100x) (c) a calcium deposit as identified with energy dispersive X-ray spectroscopy (4000x) (EDS) at 20kV (d) localized surface irregularity corresponding to the presence of sulphur and calcium as identified by EDS (7000x)

ESEM micrographs were taken and EDS spot analysis was performed on pit 2 on API X70 coupon 8 [Figure 20a, b]. Of particular significance was the discovery of relatively large calcium deposits [Figure 20c] found near regions of localized pitting and attack [Figure 20d].

These regions of interest were also located around the edge of the intact scale on the bottom of the pit.

Further microbiological analysis including cell counts, cultivations experiments and 16S rRNA gene sequencing and will be performed to characterize the microbial diversity in the corrosion cell containing coupon 8. Additional immersion tests will also be performed to reproduce and confirm the influence of microbes on the corrosion of carbon steel in environments relevant to FGE infrastructure. The impacts of other microbes cultivated from samples collected from FGE infrastructure will also be evaluated.

Electrochemical Evaluation of Steel Corrosion Parameters for E10 and Water Mixtures

To characterize the effect of water addition to ethanol fuel blends, varying concentrations of water in the range 15 to 50 pct. were added to E10 gasoline and the conductivity values of the water phase were evaluated. It is likely that ethanol transfers from E10 upon addition of water into the aqueous phase, due to the greater solubility of ethanol in water. EIS measurements were performed on A36 carbon steel specimens immersed in the water phase after water was added in the above mentioned concentration range to E10.

Figure 21 shows the polarization resistance of ASTM A36 carbon steel in water-ethanol phase and the conductivity of water-ethanol phase upon water addition to E10. It is evident from the figure that the conductivity of the aqueous phase increases with increase in water concentration to E10. The maximum change in conductivity takes place in the range 20-25 %. Polarization resistance of ASTM A36 carbon steel decreases with increase in water concentration to E10, correlating with the order of conductivity. The increase in conductivity accords with the observed increase in corrosion rate for the steel specimens.

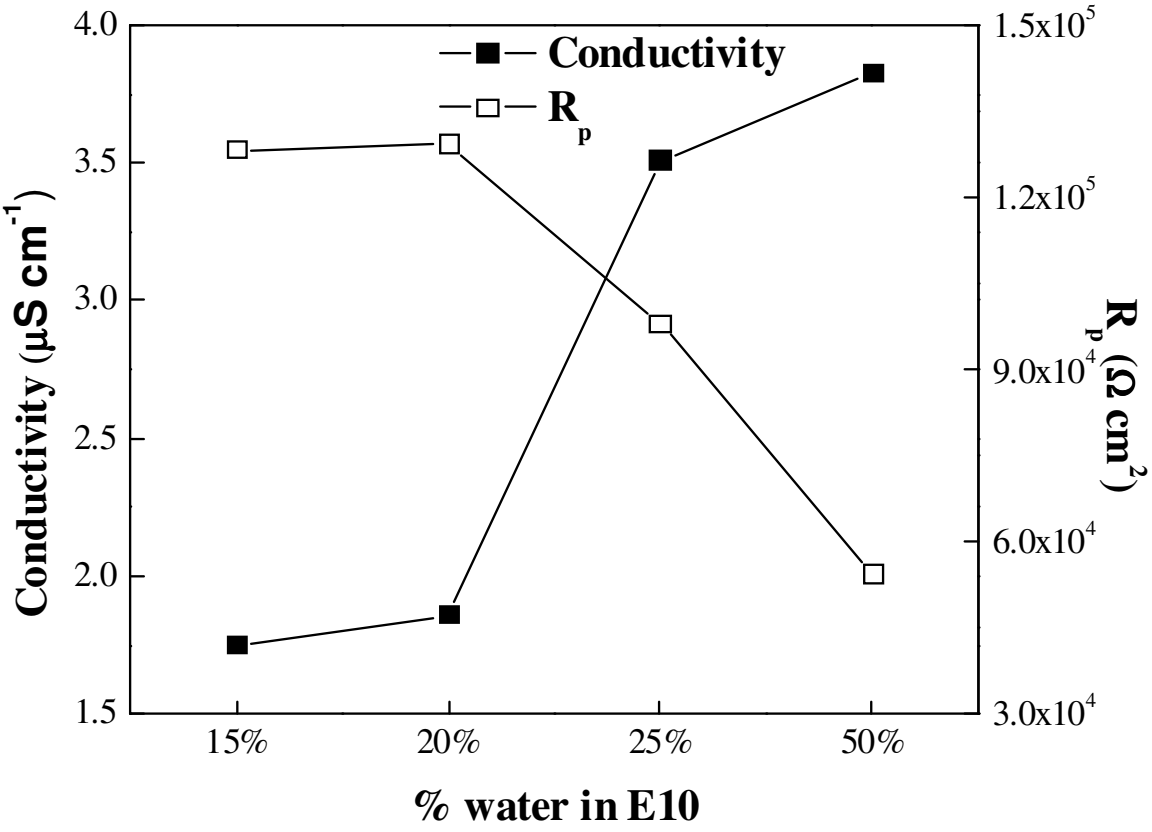

Figure 21 Polarization resistance and conductivity measurements of ASTM A36 carbon steel in the water-ethanol phase of E10 and water mixtures

Immersion testing was performed on ASTM A36 carbon steel specimens after adding water in the range mentioned above. Field emission scanning electron microscopy (FESEM) measurements were performed on the specimens after seven days of immersion. Figure 22 shows the micrograph of an ASTM A36 carbon steel coupon at 100x magnification after being immersed in gasoline-ethanol and water-ethanol phases for seven days. The top half portion of the micrograph representing the water-ethanol phase exhibits extensive corrosion while the bottom half portion of the micrograph representing the gasoline-ethanol phase displays a corrosion-free surface. The extent of corrosion was found to be the greatest near the interface in the water-ethanol phase.

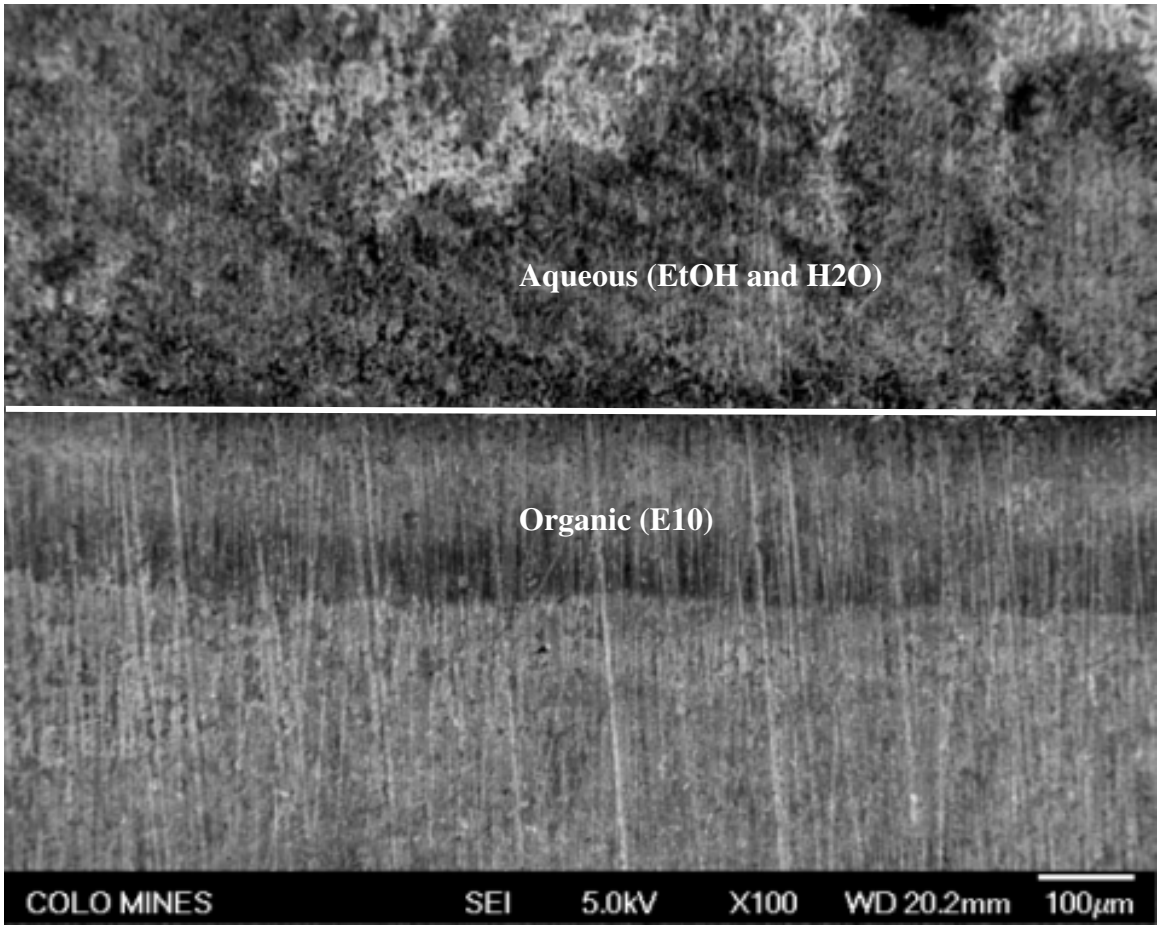

Figure 22 Field emission scanning electron microscopy (FESEM) micrograph of an ASTM A36 steel coupon magnification after being immersed in gasoline-ethanol and water-ethanol phases for seven days (100x)

Fatigue Crack Growth Rate Measurement

Fatigue crack growth rate (FCGR) tests required design of a reaction frame that allows submersion of the test specimens, while minimizing exposure of load frame components to the local fuel corrosion environments. A reaction frame was designed for this purpose as reported earlier. Detailed schematics of the FCGR reaction frame were sent to a local machine shop for fabrication. These schematics were reported in previous reports and are shown again in full mockup in Figure 23. Fabrication of these parts was completed in August and September and parts were installed this quarter on a 20,000 lb capacity servohydraulic test machine.

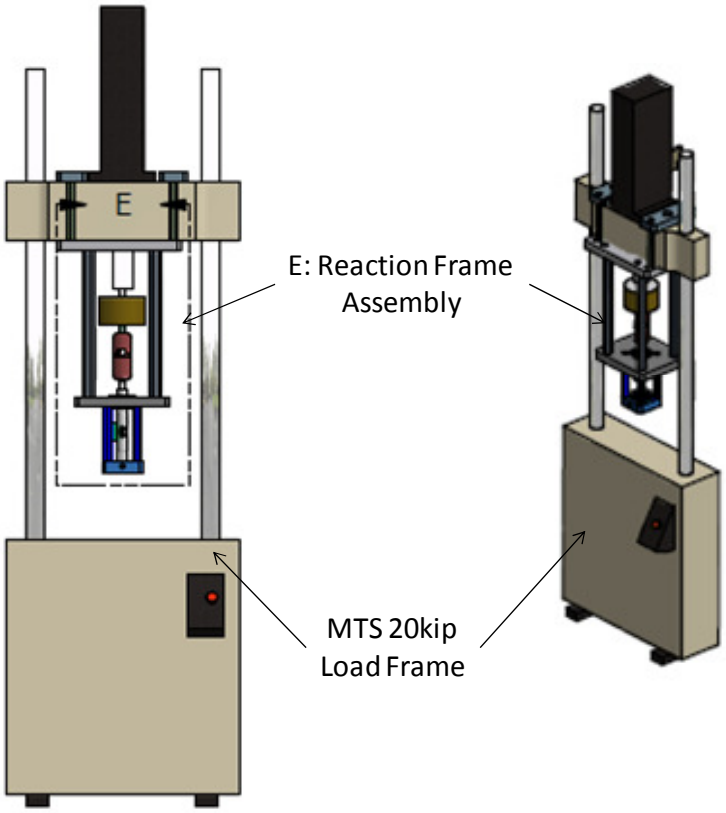

Figure 23 Solid model of reaction frame assembly generated by CAD software

The assembled and installed reaction frame is shown in Figure 24. The mechanical load cell was installed directly to the actuator to prevent contact with corrosive solutions. Beneath the load cell, a universal joint was installed in the load train. Inclusion of this feature, along with several spiral washers in series, was incorporated into the design to aid in specimen alignment.

Specimen alignment is important during fatigue testing since loading out of plane due to misalignment can result in unwanted bending that can complicate the stress state at the growing fatigue crack tip. These features will ensure that loading is performed in tension only. The placement location of the vessel containing the desired test solutions is indicated. Note that the frame is moved vertically via a servohydraulic lift-and-lock system to submerge or remove the fixture test specimens into the solutions. This design allows easy access to the environmental containment vessel.

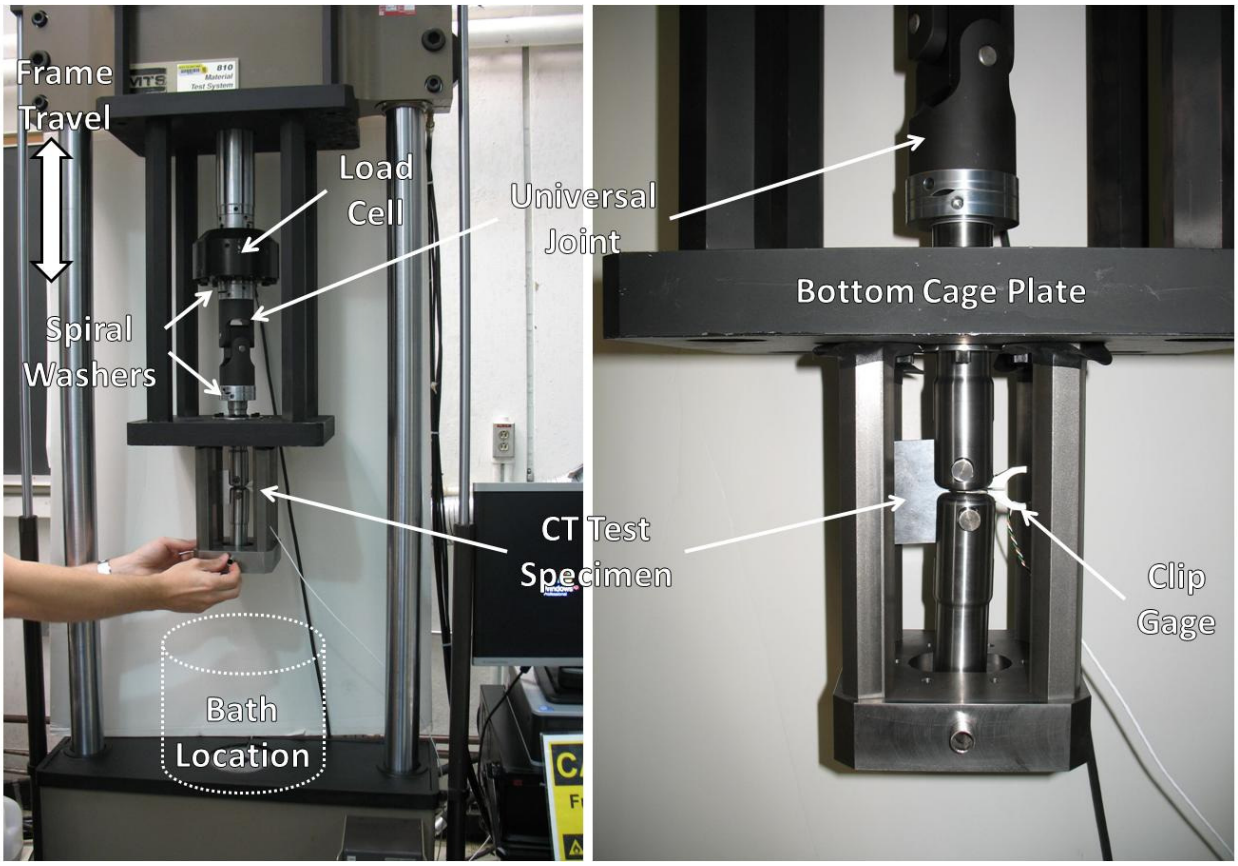

Figure 24 Images of assembled reaction frame installed on the servo-hydraulic test machine

Testing in corrosive fuel blends necessitated special consideration of materials to be incorporated into reaction frame design. Extensive use of high strength stainless steel was incorporated into the design to prevent corrosion of the reaction frame itself. All parts below the bottom cage plate were fabricated from stainless steel (S.S.) as shown in Figure 25. A Teflon film was adhered to the bottom side of the cage plate. This cage plate was fabricated from carbon steel; therefore it was necessary to apply the Teflon film to provide corrosion protection from the fuel

environments in the containment vessel placed below the cage plate. It is well known that dissimilar metal contact in corrosive environments results in galvanic corrosion. Therefore, the compact tension (CT) specimens are electrically insulated from the stainless steel clevis grips by use of ceramic loading pins (not shown) to prevent. Extensive use of vapor seals was incorporated into the design to minimize escape of evaporated test solutions from the bath. Note the top and bottom wiper seals surrounding the clevis grips. These measures should adequately contain the corrosive test solutions while minimizing damage to the frame itself.

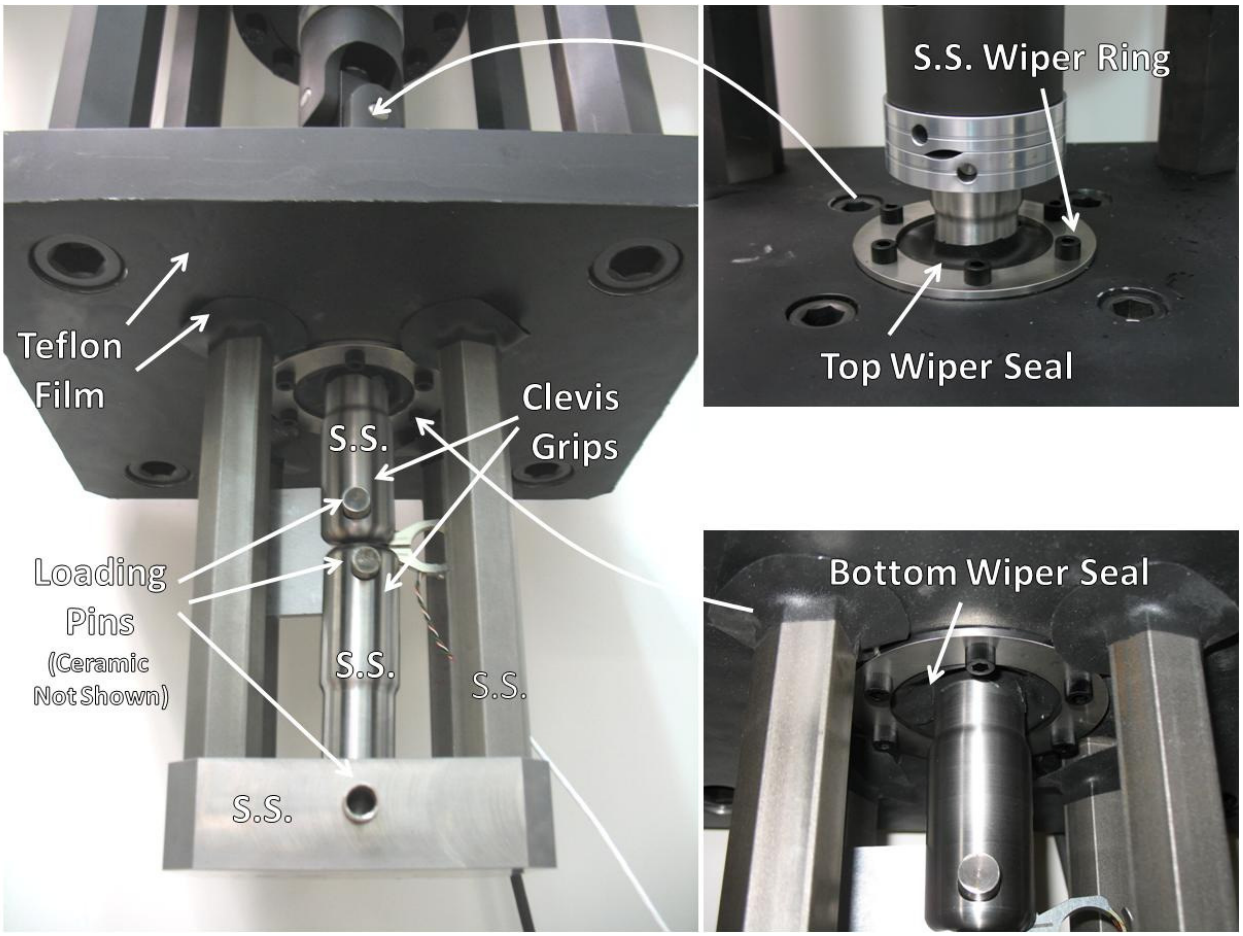

Figure 25 Images of assembled reaction frame below the bottom cage plate

Clip gages were procured from a local manufacturer that specializes in making customized high-precision measurement gages. These gages, which were specifically ordered to fit the narrow CT specimens selected for this study, are necessary for crack growth measurements. Narrow CT specimens were necessary for the current work since the materials (A36, X52, X70) were thin

walled and the maximum obtainable thickness was 0.225 in. for the three steel alloys. A clip gage installed on an ASTM A36 steel CT specimen is shown in Figure 26.

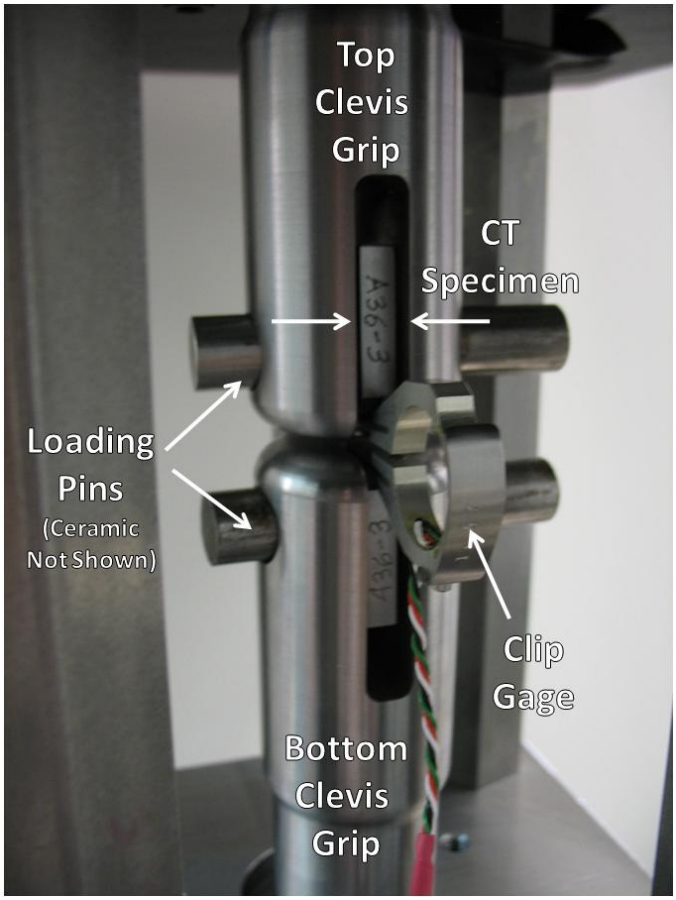

Figure 26 Image of specimen fixture region showing ASTM A36 steel CT specimen fixed in clevis grips and attached clip gage

Load calculations were determined for CT testing of steels with the specimen geometry and critical dimension for calculating stress intensity shown in Figure 27. Stress intensity was computed with these values and a variable load (P). A plot was obtained relating the applied load to the stress intensity at the crack for a crack length of 1.0 in (25.4 mm). The results are plotted in Figure 28. Note that the typical stress intensity ranges evaluated during steel FCGR measurements are indicated. Expected loads to achieve these stress intensity values are below 2,000 lbf (~8.9 kN). This load was considered peak test load during reaction frame design. Safety factor calculations were performed accordingly to ensure the frame was sufficiently rigid to complete the proposed testing.

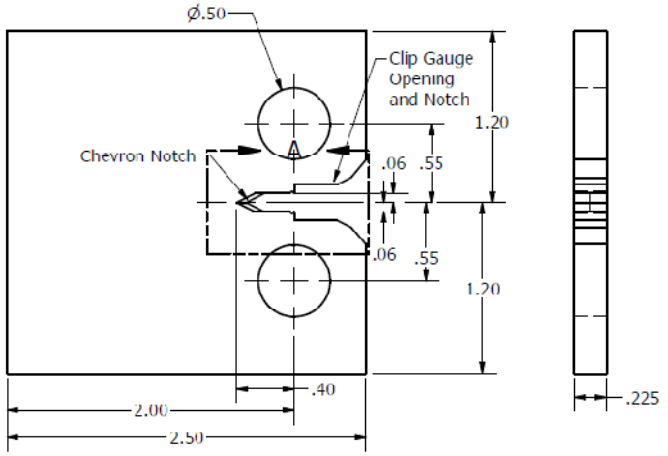

Constants	Length (in)	Length (m)
B	0.225	0.0057
W	2	0.0508
a*	1	0.0254
f	9.659	9.659

Figure 27 CT specimens fabricated for ethanol testing, and table containing critical specimen dimensions for stress intensity calculations

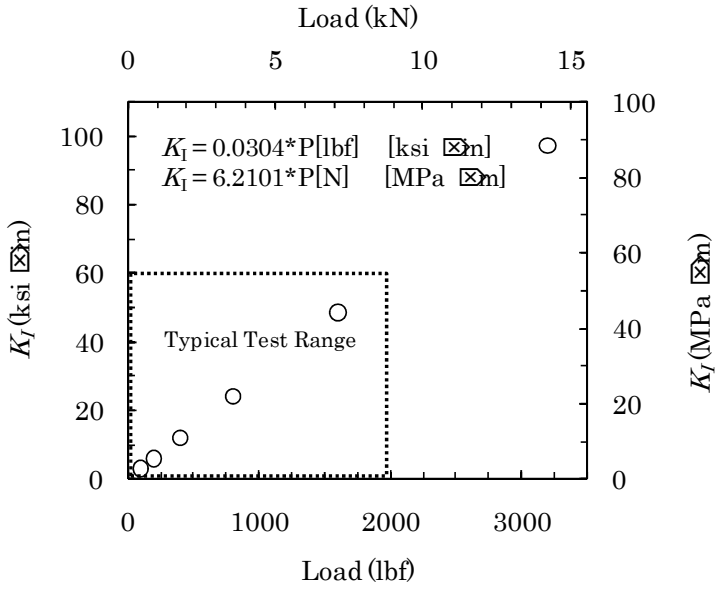

Figure 28 Relationship between applied load and stress intensity at 1.0 in (25.4 mm) initial crack length in CT specimens

Fatigue studies will be performed for the three steel alloys under ambient test conditions to characterize baseline FCGR. Characteristic fatigue crack growth rate curves (da/dN versus ΔK) will be generated in air for baseline values. It is expected that the FCGR studies will be performed at a minimum 20 Hz test frequency. These test frequencies are sufficient such that all baseline tests will take approximately two weeks to complete. It is expected that FCGR baseline

characteristics will be completed in October 2010 at which time the fuel blend testing can begin. A work timeline chart is shown in Figure 29 where time to complete FCGR experiments is estimated. It is assumed that corrosion FCGR studies will take approximately two weeks to complete. This chart allows for each of the three steel alloys to be tested in at least five solutions during the remainder of the project. The fuel blends will be selected based on results from the microbial studies.

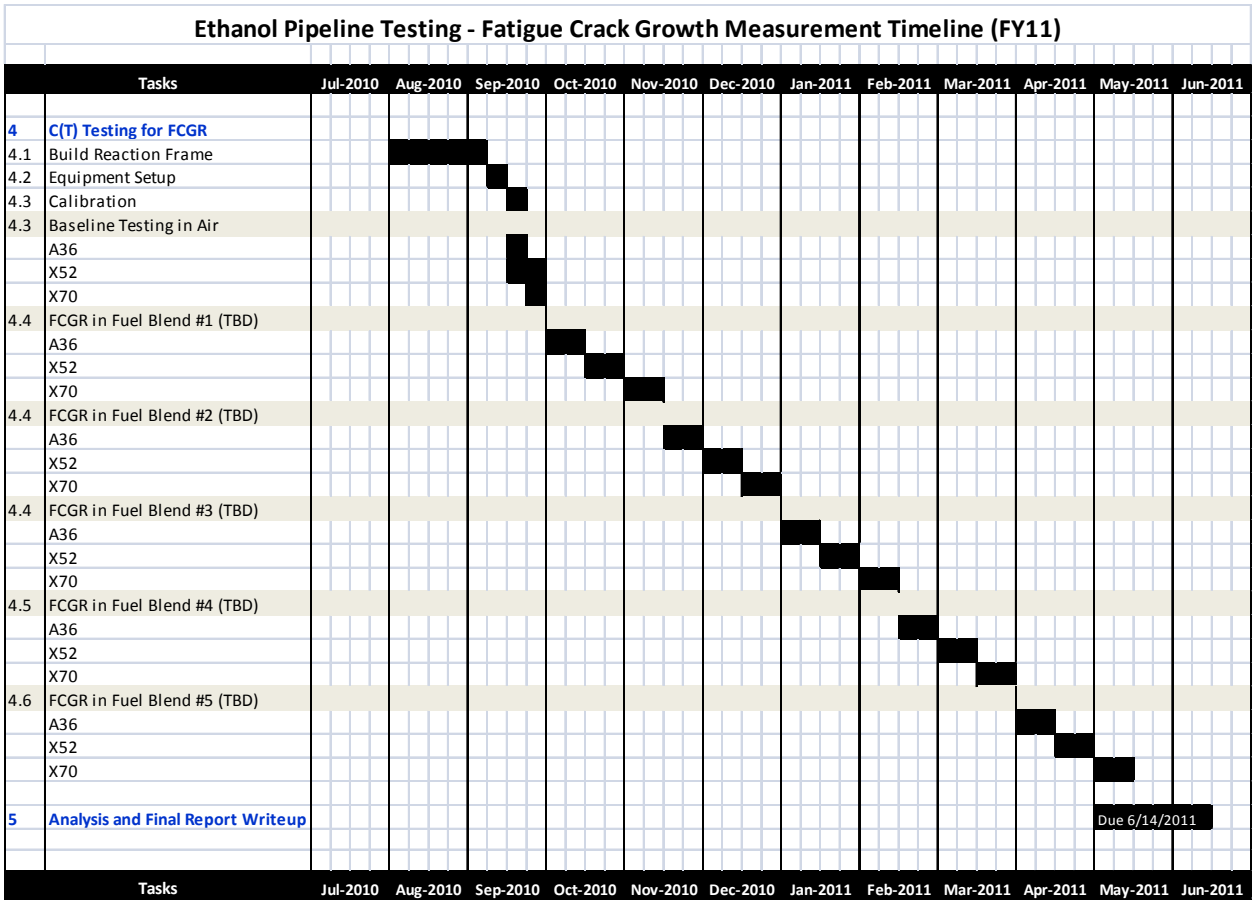

Figure 29 Timeline chart containing outlook for FCGR studies

NIST Test Safety

Fume extraction systems designed to contain and remove fuel vapors from the testing laboratory were installed and are now functional. A detailed standard operating procedure (SOP) was completed for mechanical testing in blended fuel solutions at the NIST facility. This SOP was approved by the NIST safety office and a final hazard assessment was performed. These tasks

were prerequisites to test commencement. Approval to begin testing was provided in the middle of August after all safety protocols were in place, and MSBT of ASTM A36 steel in ethanol-water solutions was initiated on August 24. The test facility now has full capability to test in all fuel solutions containing no microbial life. Once specific microbial species are selected for testing, an additional safety review will be performed so that safe procedures are in place for handling microbes at the NIST facility.

Works Cited

B. J. Little, J.S. Lee, R.I. Ray. "Diagnosing Microbiologically Influenced Corrosion: A State-of-the-Art Review." *Corrosion*, 2006: 1006.

Blackburn, Freeman E. "Non-Bioassay Techniques for Monitoring MIC. Paper 04580." *Corrosion2004.* Houston, TX: NACE International, 2004.

Javaherdashti, Reza. *Microbiologically Influenced Corrosion.* London: Springer-Verlag, 2008.

Videla, H. A. "Biofouling and Microbially Influenced Corrosion." *International Biodeterioration and Biodegradation*, 1992: 195.

RESULTS AND CONCLUSIONS:

- Analyses of samples collected from fueling terminals handling fuel grade ethanol have continued. DNA sequencing suggests that microbes with metabolisms that may increase corrosion are present in ethanol fuel industry infrastructure.
- Microbial growth and corrosion experiments have continued to determine the ability of microbes to affect corrosion in high-ethanol environments.
- Viable microbes have been cultivated from a variety of ethanol fuel industry infrastructure samples, including samples collected from fuel grade ethanol environments containing less than one percent water. These experiments suggest that viable microbes potentially capable of increasing corrosion of steels are present in environments containing fuel grade ethanol.
- MIC has most likely been observed on API X70 steel coupons in an E10 and water mixture using microbes acquired from active ethanol fuel infrastructure
- Electrochemical corrosion parameters have been measure for E10 and water mixtures in the range of 15 to 50 pct. water
- An FCGR reaction frame has been assembled for evaluation of MIC in ethanol fuel environments
- Safe operating procedures have been established for testing in fuel at NIST, Boulder

PLANS FOR FUTURE ACTIVITY:

- Continue experiments to determine the ability of microbes, including spores, to affect corrosion in high-ethanol environments.
- Pursue sampling opportunities and collect samples from EFB infrastructure.
- Continue experiments to isolate viable microbes from EFB infrastructure samples.
- Test the affect of environmentally relevant cultivars and cultivars isolated from EFB infrastructure on corrosion of steel using immersion specimens
- Test the affect of environmentally relevant cultivars and cultivars isolated from EFB infrastructure on corrosion of steel using bending specimens
- Test the affect of environmentally relevant cultivars and cultivars isolated from EFB infrastructure on corrosion of steel using CT specimens